miR147b: A novel key regulator of interleukin 1 beta-mediated inflammation in human astrocytes

van Scheppingen, J.; Mills, J.D.; Zimmer, T.S.; Broekaart, D.W.M.; Iori, V.; Bongaarts, A.; Anink, J.J.; Iyer, A.M.; Korotkov, A.; Jansen, F.E.; van Hecke, W.; Spliet, W.G.; van Rijen, P.C.; Baayen, J.C.; Vezzani, A.; van Vliet, E.A.; Aronica, E.

DOI
10.1002/glia.23302

Publication date
2018

Document Version
Author accepted manuscript

Published in
GLIA

miR147b: a novel key regulator of interleukin 1 beta-mediated inflammation in human astrocytes

Journal:	*GLIA*
Manuscript ID	GLIA-00378-2017.R2
Wiley - Manuscript type:	Original Research Article
Date Submitted by the Author:	11-Jan-2018
Complete List of Authors:	van Scheppingen, Jackelien; University of Amsterdam, Department of (Neuro)Pathology, Academic Medical Center Mills, James; University of Amsterdam, Department of (Neuro)Pathology, Academic Medical Center Zimmer, Till; University of Amsterdam, Department of (Neuro)Pathology, Academic Medical Center Broekaart, Diede; University of Amsterdam, Department of (Neuro)Pathology, Academic Medical Center Iori, Valentina; Istituto Di Ricerche Farmacologiche Mario Negri, Neuroscience Bongaarts, Anika; University of Amsterdam, Department of (Neuro)Pathology, Academic Medical Center Anink, Jasper; University of Amsterdam, Department of (Neuro)Pathology, Academic Medical Center Iyer, Anand; University of Amsterdam, Department of (Neuro)Pathology, Academic Medical Center Korotkov, Anatoly; University of Amsterdam, Department of (Neuro)Pathology, Academic Medical Center Jansen, Floor; Universitair Medisch Centrum Utrecht, Department of Pediatric Neurology van Hecke, Wim; Universitair Medisch Centrum Utrecht, Department of Pathology Spliet, Wim; Universitair Medisch Centrum Utrecht, Department of Pathology van Rijen, Peter; UMC Utrecht Hersencentrum Rudolf Magnus, Department of Neurosurgery Baayen, Johannes; VU University Medical Center, Department of Neurosurgery Vezzani, Annamaria; Mario Negri Institute for Pharmacological Research, Neuroscience van Vliet, Erwin; University of Amsterdam, Department of (Neuro)Pathology, Academic Medical Center Aronica, Eleonora; Univ. of Amsterdam,
Key Words:	microRNA, inflammation, astrocytes, interleukin 1 beta, epilepsy

miR147b: a novel key regulator of interleukin 1 beta-mediated inflammation in human astrocytes

Running title: miR147b in human astrocytes

Jackelien van Scheppingen, MSc[1], James D. Mills, PhD[1], Till S. Zimmer, MSc[1], Diede W.M. Broekaart, MSc[1], Valentina Iori, MSc[2], Anika Bongaarts, MSc[1], Jasper J. Anink, BSc[1], Anand M. Iyer, PhD[1], Anatoly Korotkov, MSc[1], Floor E. Jansen, MD PhD[3], Wim van Hecke, MD[4], Wim G. Spliet, MD[4], Peter C. van Rijen, MD[5], Johannes C. Baayen, MD[6], Annamaria Vezzani, PhD[2], Erwin A. van Vliet, PhD[1]*, Eleonora Aronica, MD PhD[1,7]*

[1]*Department of (Neuro)Pathology, Academic Medical Center, University of Amsterdam, Amsterdam, The Netherlands*
[2]*Department of Neuroscience, IRCCS-Istituto di Ricerche Farmacologiche "Mario Negri", Milano, Italy*
[3]*Department of Pediatric Neurology, University Medical Center Utrecht, Utrecht, The Netherlands*
[4]*Department of Pathology, University Medical Center Utrecht, Utrecht, The Netherlands*
[5]*Department of Neurosurgery, Rudolf Magnus Institute for Neuroscience, University Medical Center Utrecht, Utrecht, The Netherlands*
[6]*Department of Neurosurgery, VU University Medical Center, Amsterdam, The Netherlands*
[7]*Stichting Epilepsie Instellingen Nederland (SEIN), The Netherlands*

* contributed equally.

Correspondence should be addressed to:
Dr. E. Aronica
University of Amsterdam,
Academic Medical Center,
Dept. (Neuro) Pathology,
Meibergdreef 9,
1105 AZ Amsterdam, The Netherlands
Phone: +31 20 5662943
FAX: +31 20 5669522
E-mail: e.aronica@amc.uva.nl

Acknowledgements

The research leading to these results has received funding from the European Union's Seventh Framework Programme (FP7/2007-2013) under grant agreement no. 602391 (EPISTOP; J.v.S., E.A., F.E.J.) and no. 602102 (EPITARGET; E.A., E.A.v.V., A.V.), the Dutch Epilepsy Foundation, project number 13-01 (E.A., V.I., A.V.) and 16-05 (D.W.M.B., E.A.v.V.) and the European Union's Horizon 2020 Research and Innovation Programme under the Marie Sklodowska-Curie grant agreement no. 642881 (ECMED; A.K., E.A.) and no. 722053 (EU-GliaPhD; T.S.Z., E.A.). We acknowledge the HIS Mouse Facility of the Academic Medical Center, Amsterdam and the Bloemenhove Clinic (Heemstede, The Netherlands) for providing fetal tissues.

Conflict of interest

Nothing to report (for all authors).

Word count: *(including references)*
Body of manuscript: 4999 words
Abstract: 248 words
Introduction: 565 words
Materials and Methods: 1577 words
Results: 1106 words
Discussion: 1745 words
Bibliography: 1378 words
Figure legends: 1082

Abstract

Astrocytes are important mediators of inflammatory processes in the brain and seem to play an important role in several neurological disorders, including epilepsy. Recent studies show that astrocytes produce several microRNAs, which may function as crucial regulators of inflammatory pathways and could be used as therapeutic target. We aim to study which miRNAs are produced by astrocytes during IL-1β mediated inflammatory conditions *in vitro*, as well as their functional role and to validate these findings in human epileptogenic brain tissue.

Sequencing was used to assess miRNA and mRNA expression in IL-1β-stimulated human fetal astrocyte cultures. miRNAs were overexpressed in cell cultures using miRNA mimics. Expression of miRNAs in resected brain tissue from patients with tuberous sclerosis complex or temporal lobe epilepsy with hippocampal sclerosis was examined using in situ hybridization.

Two differentially expressed miRNAs were found: miR146a and miR147b, which were associated with increased expression of genes related to the immune/inflammatory response. As previously reported for miR146a, overexpression of miR147b reduced the expression of the pro-inflammatory mediators IL-6 and COX-2 after IL-1β stimulation in both astrocyte and tuberous sclerosis complex cell cultures. miR146a and miR147b overexpression decreased proliferation of astrocytes and promoted neuronal differentiation of human neural stem cells. Similarly to previous evidence for miR146a, miR147b was increased expressed in astrocytes in epileptogenic brain.

Due to their anti-inflammatory effects, ability to restore aberrant astrocytic proliferation and promote neuronal differentiation, miR146a and miR147b deserve further investigation as potential therapeutic targets in neurological disorders associated with inflammation, such as epilepsy.

Key words: microRNA; inflammation; astrocytes; interleukin 1 beta; tuberous sclerosis complex; temporal lobe epilepsy.

Main points:

- miR146a and miR147b are up-regulated in fetal astrocytes after IL-1β stimulation.
- miR147b inhibits inflammation and aberrant astrocytic proliferation, promotes neuronal differentiation and is up-regulated in astrocytes in human epileptogenic brain.

Introduction

A dysregulated inflammatory response is present in various pathologies of the central nervous system (CNS), including epilepsy, which is one of the most common chronic neurological disorders, affecting more than 50 million people worldwide. In the epileptogenic brain, astrocytes, which are abundantly present, are considered one of the most important type of glial cells contributing to the neuroinflammatory response (Aronica et al. 2012; Vezzani et al. 2011). Astrocytes can produce various pro-inflammatory mediators, including cytokines and chemokines, which leads to activation of the innate and adaptive immune response (Colombo and Farina 2016; Farina et al. 2007; Vezzani et al. 2011). Reactive gliosis in epilepsy is also characterized by increased proliferation and aberrant generation of astrocytes from progenitor cells (Sierra et al. 2015; Sofroniew and Vinters 2010). *In vitro*, this increased proliferation can be induced by treatment with the pro-inflammatory cytokine interleukin-1β (IL-1β) (Cui et al. 2011), which is a key player in neuroinflammation, and is mainly produced by activated **astro**glial cells in response to tissue damage, increased neuronal activity (Xanthos and Sandkuhler 2014) or cellular stress (Moynagh 2005; Ravizza et al. 2008; Srinivasan et al. 2004). IL-1β is also highly expressed both in experimental rodent models of epilepsy and in human epileptogenic brain and contributes to seizure generation and epileptogenesis in animal models (Vezzani et al. 2011). Among its cellular targets, IL-1β acts on astrocytes by activating the IL-1 receptor (IL-1R1), thus leading to NF-κB-mediated transcription of growth factors and various immune-related molecules including cytokines and danger signals (Aronica et al. 2017; Sparacio et al. 1992).

Previous studies indicate that astrocytes also produce a family of microRNAs (miRNAs), small non-coding RNAs that are post-transcriptional regulators of gene expression, which are crucial modulators of inflammatory pathways linked to various neurological disorders, including epilepsy (Li et al. 2010). The expression of several miRNAs, including those associated with neuroinflammatory signals,

has been shown to change in human epilepsy and experimental models of epilepsy, providing either targets for treatment or valuable disease biomarkers (Gorter et al. 2014; Li et al. 2014). For example, it was previously reported that miR146a, which is associated with modulation of IL-1R/Toll like receptor 4 signaling, is up-regulated in several CNS pathologies including epilepsy, and serves as an important feedback inhibitor of inflammation in astrocytes (Aronica et al. 2010; Iyer et al. 2012; van Scheppingen et al. 2016b). Recently, it has been shown that administration of miR146a in mice developing epilepsy prevented disease progression and reduce seizures (Iori et al. 2017), indicating that miRNAs related to neuroinflammation could have therapeutic value in epilepsy.

Besides miR146a, there may be other miRNAs that could have therapeutic potential. In order to identify these miRNAs, high throughput, transcriptome wide studies are required. To the best of our knowledge no such study has been performed yet in human astrocytes. Therefore, we studied which miRNAs are produced by **fetal** human astrocytes during inflammatory conditions *in vitro* and validated these findings in human epileptogenic brain tissues, in two different epilepsy associated pathologies: Tuberous Sclerosis Complex (TSC; a genetic disorder with focal developmental malformations of the cerebral cortex) and Temporal Lobe Epilepsy with hippocampal sclerosis (TLE-HS; the most common type of symptomatic epilepsy in adults). In addition, we investigated the functional role of two miRNAs, which were differentially expressed by astrocytes upon IL-1β/IL-1R1 activation, on the expression of inflammatory mediators, proliferation and differentiation of **fetal** human astrocytes and neural stem cells in culture.

Materials and methods

Astrocyte and tuberous sclerosis complex cell cultures

Primary **fetal** astrocyte-enriched cell cultures were obtained from human fetal brain tissue (cortex, 14-19 gestational weeks) obtained from medically induced abortions. All material has been collected from donors from whom a written informed consent for the use of the material for research purposes had been obtained by the Bloemenhove clinic. Tissue was obtained in accordance with the Declaration of Helsinki and the Academic Medical Center (AMC) Research Code provided by the Medical Ethics Committee of the AMC. Cell isolation was performed as described previously ((van Scheppingen et al. 2016b) see supplementary material). TSC cell cultures were derived from surgical brain specimens obtained from 2 patients (age at surgery: 2.5 and 2 years; gender: male; mutation: TSC2) undergoing epilepsy surgery at the Wilhelmina Children's Hospital of the University Medical Center Utrecht (UMCU, Utrecht, The Netherlands). TSC cultures were established in the same manner as fetal cultures.

Neural stem cell cultures

Neural stem cells (NSCs) were obtained from fetal brain (14-16 gestational weeks). Tissue was enzymatically digested by incubating at 37˚C for 30 minutes with 0.3% trypsin (Sigma-Aldrich; St. Louis, MO, USA). The reaction was stopped by the addition of fetal calf serum (FCS). Cells were washed and taken up in complete deficient medium (dDMEM; DMEM without phenol with 10% FCS and 1% P/S) and triturated through a 70 µm mesh filter. NSCs were selected by a five-step discontinuous density gradient separation. 100% standard isotonic Percoll (SIP, 9 parts Percoll, GE Healthcare, Auckland, New Zealand, with 1 part 10x PBS pH 4.6) was diluted to 50, 40, 30, 20 and 10% with dDMEM and these dilutions were

layered starting with the highest concentration at the bottom and the cells on top. After centrifugation, the cells at the 30/40% SIP interphase were collected and grown at 37˚C, 5% CO_2 in proliferative medium (DMEM/HAM F10 (1:1) supplemented with 2% B27 (50x), 20 ng/ml EGF, 20 ng/ml bFGF (all from Gibco, Thermo Fisher Scientific, Waltham, MA, USA), 1% P/S). Medium with EGF and bFGF was refreshed every 2-3 days. For transfection and differentiation experiments, NSCs were re-plated on laminin (10 µg/ml, Sigma-Aldrich). For differentiation of NSCs, medium was replaced by DMEM/HAM F10 (1:1) with 1% P/S and 5% FCS. To quantify differentiation, βIII-tubulin positive cells were counted , and the number of 4',6-diamidino-2-phenylindole (DAPI) positive nuclei was determined with particle analysis (both with ImageJ 1.44p, National Institutes of Health, Bethesda, MD, USA).

Transfection and stimulation of cell cultures

Cells were transfected with mimic pre-miRNA for miR146a or miR147b (mirVana miRNA mimics, Applied Biosystems, Carlsbad, CA, USA) for 24 hours as described previously (van Scheppingen et al. 2016b). Astrocyte cultures were stimulated with human recombinant (r)IL-1 β (10 ng/ml; Peprotech, Rocky Hill, NJ, USA) or lipopolysaccharide (LPS; 100 ng/ml; Sigma, St. Louis, MO, USA) for 24 hours. Viability of human cell cultures was not influenced by the treatments (as shown previously; (van Scheppingen et al. 2016a)). To examine the effect of the IκB kinase-2 (IKK-2) inhibitor TPCA-1 in astrocyte cultures, treatment with 1 or 5 µM TPCA-1 (Selleck Chemicals, Munich, Germany) in DMSO (0.05% final DMSO concentration) was started 1 hour before stimulation with IL-1β was initialized, and treatment was continued during stimulation.

RNA isolation

For RNA isolation, cell culture or fresh brain tissue was homogenized in Qiazol Lysis Reagent (Qiagen Benelux, Venlo, The Netherlands). Total RNA was isolated using the miRNeasy Mini kit (Qiagen Benelux, Venlo, The Netherlands) according to manufacturer's instructions. The concentration and purity of RNA were determined at 260/280 nm using a NanoDrop 2000 spectrophotometer (Ocean Optics, Dunedin, FL, USA).

RNA-Sequencing

RNA-Sequencing (RNA-Seq) was performed on control and IL-1β stimulated fetal astrocytes (n = 5 donors). Two different RNA-Seq techniques were used; mRNA-Seq to identify transcripts of ~180 nucleotides in length and longer, and small RNA-Seq to identify transcripts shorter than ~50 nucleotides. Library preparation and sequencing was completed by GenomeScan (Leiden, the Netherlands) as described previously (Mills et al. 2017).

Bioinformatics analysis of small RNA and mRNA-Seq data

mRNA-Seq data was analyzed as previously described (Mills et al. 2017). For small RNA-Seq, read quality was assessed using FastQC v0.11.2 software (Babraham Institute, Cambridgeshire, UK) and Trimmomatic v0.36 was used to filter reads of low quality (Bolger et al. 2014). See supplementary material for details.

Gene ontology and pathway enrichment analysis

The Database for Annotation, Visualization and Integrated Discovery (DAVID) version 6.8 (http://david-d.ncifcrf.gov) was used to test DEGs for gene ontology (GO) and pathway enrichment (Huang da et al.

2009). GO terms and pathways with a Benjamini-Hochberg corrected p-value<0.05 were considered enriched. The enriched pathway list produced by DAVID, was processed using Cytoscape (http://www.cytoscape.org/) to produce a visual output of the text-based pathway list (Cline et al. 2007).

Real-time quantitative PCR and ELISA

Expression of miR146a, miR147b, and the reference genes miR23a (for extracellular miRNA) and the small-nucleolar RNAs RNU6B and RNU44 (for cellular miRNA) was analyzed using Taqman MicroRNA assays (Applied Biosystems, Foster City, CA, USA). cDNA was generated using Taqman MicroRNA reverse transcription kit (Applied Biosystems, Foster City, CA, USA). mRNA expression was evaluated as described previously (van Scheppingen et al. 2016b), using EF1A and C1orf43 as reference genes.

Levels of IL-6 were measured in culture supernatants using the PeliKine Compact™ IL-6 ELISA kit (Sanquin, Amsterdam, the Netherlands) according to the manufacturer's instructions.

Immunocytochemistry

Immunocytochemistry on cells was performed as described previously (van Scheppingen et al. 2016a) using the following primary antibodies: Ki67 (clone MIB-1, monoclonal mouse, DAKO, Glostrup, Denmark, 1:200); βIII-tubulin/Tuj1 (monoclonal mouse, Neuromics, Edina, MN, USA, 1:6000); Glial fibrillary acidic protein (GFAP, polyclonal rabbit, DAKO, 1:2000); SRY (sex determining region Y)-box 2 (SOX2, polyclonal rabbit, Millipore, Darmstadt, Germany, 1:1000); Nestin (monoclonal mouse, R&D, Minneapolis, MN, USA, 1:500) and the following secondary antibodies or counterstaining: Alexa Fluor® 488 donkey-anti-mouse antibody (Invitrogen, Eugene, OR, USA, 1:200); Alexa Fluor® 568 goat-anti-rabbit antibody (Invitrogen, 1:200); Alexa Fluor® 594 Phalloidin (Life Technologies, 1:200, Eugene, OR, USA).

Coverslips were mounted with Vectashield with DAPI (H-1200, Vector Laboratories Inc., Burlingame, CA, USA). Fluorescent microscopy was performed using Leica Confocal Microscope TSC SP-8X (Leica, Son, the Netherlands).

Proliferation assay

Proliferation of cell cultures was determined 72 hours after start of transfection by cell cycle flow cytometric analysis and Ki67 staining. Ki67 positive cells and the total number of DAPI-stained nuclei were manually counted with ImageJ (1.44p, National Institutes of Health, Bethesda, MD, USA). For each culture, conditions were plated in triplicate and fifteen fields per coverslip, with on average 1100-1300 cells per condition, were counted using a 20x magnification objective. Staining was evaluated with a Leica DM5000B fluorescence microscope equipped with a Leica DFC 500 camera and Leica Application Suite X software (Leica Microsystems CMS GmbH, version 1.5.1, Wetzlar, Germany). The number of Ki67 positive cells was compared with the number of DAPI nuclei to determine the percentage of proliferating cells.

For flow cytometric cell cycle analysis, cells were suspended in PBS/1% BSA and stained with Fixable Viability Dye eFluor® 780 (eBioscience, San Diego, CA, USA) on ice for 30 minutes. After fixation with 100% ethanol, cells were incubated with Propidium Iodide (1:100, Life Technologies) and RNAse A (1 g/ml used 1:1000, Sigma-Aldrich) in PBS for 10 minutes at 37˚C. Flow cytometric analysis of stained cells was performed using a FACSCanto Flow Cytometer equipped with FACSDiva software (BD Biosciences, San Jose, CA, USA) and data analysis was performed using FlowJo 7.6 (FlowJo LLC, Ashland, OR, USA). Viable cells showing a DNA content between G1 and G2 (S-phase) were selected as proliferative population.

Human material

The cases included in this study were obtained from the archives of the departments of neuropathology of the AMC, the UMCU, VU Medical Center Amsterdam (The Netherlands), Motol University Hospital (Prague, Czech Republic) and Medical University Vienna (Austria). We evaluated 22 TSC and 16 TLE-HS patients from whom we obtained anatomically well preserved epileptogenic brain tissue and sufficient clinical data (TSC: 19 surgical specimens and 3 autopsy specimens; mean age at resection = 16.7 years; standard deviation (SD)= ± 14.46 years; range = 0.83-47 years; localization: 15 frontal, 6 temporal, 1 parietal; 12 males, 10 females; TSC1/TSC2 mutation status 5/17; mean duration of epilepsy: 13.7 ± 12.7 years; seizures >5/day. TLE-HS: 16 surgical specimens, mean age at resection = 39 years ± 12 years; range = 24-66 years; localization: hippocampal; 9 males, 7 females; mean duration of epilepsy: 20 ± 12 years; seizures: 13/month). The age- and localization-matched control group consisted of 31 autopsy cases of which 17 cortex (male/female: 7/10; years/range: 0.2-48; frontal:/temporal/parietal: 9/7/1) and 14 hippocampal (male/female: 9/5; years/range: 25-86). None of these patients had a history of seizures or other neurological diseases. Tissue was obtained and used in accordance with the Declaration of Helsinki and the AMC Research Code provided by the Medical Ethics Committee. The local ethical committees of all participating centers gave permission to undertake the study.

In situ hybridization

In situ hybridization (ISH) for miR147b was performed on 5 µm thick tissue sections using a double digoxygenin (DIG)-labeled probe (with LNA modification every third nucleotide, Exiqon, Vedbaek, Denmark) as described previously (van Scheppingen et al. 2016b).

Statistical analysis

Statistical analysis of cell culture experiments was performed with GraphPad Prism® software (Graphpad software Inc., La Jolla, CA, USA) using the non-parametric Mann-Whitney U test or, for multiple groups, the non-parametric Kruskall-Wallis test with correction for multiple comparisons (Dunn's method). Correlations were assessed with SPSS (IBM Corp., Armonk, NY, USA) using the Spearman's rank correlation test. $P<0.05$ was assumed to indicate a significant difference.

Results

Small RNA-Sequencing

To explore changes in small non-coding RNA expression in astrocytes after IL-1β-stimulation, small RNA-Seq was carried out on control and IL-1β stimulated **fetal** astrocyte cultures. Each sequencing run produced ~11 million paired-end reads per sample. After quality assessment and filtering, ~7.5 million paired-end reads remained for each sample, of which ~65% were mapped to the genomic locations of various small RNA species. The expression of 881 small RNAs species across the control and IL-1β stimulated cultures was detected, this included 518 miRNAs and 295 small nucleolar RNAs. Of these 881 small RNAs, two miRNAs, miR147b and miR146a, were identified as differentially expressed and up-regulated 3.78-fold (adjusted p-value<0.033) and 5.35-fold (adjusted p-value<0.0008), respectively, in IL-1β stimulated cultures (Fig 1A).

mRNA-Sequencing

mRNA-Seq was carried out on the same set of samples that underwent small RNA-Seq. Each sample was sequenced to the depth of ~21 million paired-end reads. Overall ~16 million passed quality assessment and filtering, of which ~84% were concordantly mapped to the human reference genome GRCh38. Overall, there were 79 differentially expressed genes (DEGs); 71 genes were up-regulated in IL-1β stimulated cultures (adjusted p-value<0.05), while 8 were down-regulated after IL-1β stimulation (adjusted p-value<0.05, Fig 1B, Supp. Table 2).

A GO enrichment analysis of the 79 DEGs revealed 16 significantly enriched GO terms (adjusted p-value<0.05) across the categories biological process, cellular compartment and molecular function (Fig

1C, Table 1). The subsequent pathway enrichment analysis identified enriched pathways related to immune response and inflammation, including cytokine-cytokine receptor interaction and numerous viral infection pathways (Fig 1D, Table 2).

Positive and negative correlations were calculated between miR147b and the DEGs. The strongest correlation seen was between the expression of miR147b and the expression of C15orf48 (ρ = 0.96, $p<0.0001$, Supp. Fig 1). On closer inspection of the C15orf48 locus, it was found that the pre-miRNA of miR147b is transcribed from a region within the 3' UTR of C15orf48. C15orf48 was up-regulated 30-fold in IL-1β stimulated cultures (adjusted p-value<0.02).

miR147b and inflammatory mediators in fetal astrocyte cell cultures

In order to validate miRNA sequencing results, **fetal** astrocyte cultures were stimulated with IL-1β, and miR147b expression was evaluated at different time points. miR147b was up-regulated after IL-1β stimulation with peak expression at 30 hours ($p<0.0001$, Fig 2A), but not after stimulation with LPS. miR147b could not be detected extracellularly. Previously, we showed that miR146a expression was increased after IL-1β stimulation (van Scheppingen et al. 2016b). Pre-treatment with TPCA-1 dose-dependently reversed the up-regulation of miR146a ($p<0.0001$ for both 1 and 5 μM TPCA-1) and miR147b ($p=0.0315$ for 5 μM TPCA-1) after IL-1β stimulation (Fig 2B).

In order to examine the functional role of miR147b in astrocytes, cells were transfected with miR147b mimic, which led to an increase of expression as determined with qPCR ($p<0.0001$). miR147b overexpression led to reduced interleukin 6 (IL-6) and cyclooxygenase-2 (COX-2) mRNA expression levels after IL-1β stimulation by approximately 71 and 79%, respectively ($p=0.0002$ and $p<0.0001$ respectively, Fig 2C). IL-6 mRNA levels were also reduced by miR147b mimic under basal conditions, without IL-1β stimulation ($p=0.0002$). Transfection with miR147b mimic also reduced complement component 3 (C3)

by approximately 35% ($p<0.0001$). Enzyme-Linked Immuno Sorbent Assay (ELISA) showed reduced IL-6 on protein level after transfection with miR147b mimic, both under basal conditions and after stimulation with IL-1β ($p<0.0001$, Fig 2D). After consultation of the online databases mirDB, targetScan and DIANA tools and based on previous literature (Chatterjee et al. 2014), disintegrin and metalloproteinase domain-containing protein 15 (ADAM15), DEP domain-containing mTOR-interacting protein (DEPTOR) and interleukin 32 (IL-32) were selected as potential targets for further investigation. Of both DEPTOR and ADAM15 mRNA levels were reduced after miR147b overexpression ($p<0.0001$ and $p=0.0004$ respectively, Fig 2E), both under basal and inflammatory conditions. IL-32 showed a trend towards reduced expression (data not shown).

Altered proliferation rate after miRNA mimic transfection

Fetal astrocyte proliferation was decreased after transfection with miR146a ($p=0.0022$) and miR147b mimics ($p=0.0022$), as determined by Ki67 staining (Fig 3 A and B). Flow cytometric analysis of PI staining confirmed these results, as the percentage of cells in the S-phase was decreased after transfection with either miR146a ($p=0.0043$) or miR147b mimic ($p=0.015$, Fig 3C).

Altered neural stem cell differentiation after miRNA transfection

NSCs were grown in floating conditions and secondary cultures could be generated after dissociation (Fig 4 A and B). NSCs were positive for stem cell markers Nestin and SOX-2 and gained positivity for neuronal or astrocytic markers (βIII-tubulin and GFAP, respectively) after differentiation for 7 or 14 days (Fig 4 C-O).

The effects of miR146a and miR147b on neuronal versus astroglial cell fate differentiation in NSCs was investigated using staining for βIII-tubulin and GFAP. The βIII-tubulin/total cell count ratio was increased after transfection with miR146a ($p=0.0043$) and miR147b mimics ($p=0.0022$, Fig 5 A-M). In order to elucidate possible mechanisms, mRNA expression levels of several potential targets were examined (Fig 5 N-O). Transfection with miR146a mimic led to decreased expression of Notch homolog 1, translocation-associated protein (NOTCH1, $p=0.0260$), miR147b mimic transfection decreased the expression of both NOTCH1 ($p=0.0152$,) and Janus kinase 2 (JAK2, $p=0.0173$). We also examined expression levels of the pro-neurogenesis signaling components brain-derived neurotrophic factor, paired box protein Pax-6 and sex determining region Y-box 4, which were predicted to be regulated by miR147b. However, the expression of these genes was not altered (data not shown).

miR147b expression in tuberous sclerosis complex cortical tubers and temporal lobe epilepsy with hippocampal sclerosis

Expression and localization of miR147b in TSC and TLE-HS brain tissue was examined with qPCR of fresh brain tissue and ISH (Fig 6 A-H), respectively. miR147b expression was increased 3.5-fold in TLE-HS ($p<0.0001$, Supp. Fig 2), and in a subset of TSC tuber homogenates (n=4 out of 16, ranging from 2.1-4.2-fold increase, Supp. Fig 2). ISH showed neuronal expression of miR147b in control cortex and hippocampus. In TSC cortex miR147b expression was localized in dysmorphic neurons, giant cells and astrocytes in the tuber (co-localization with GFAP is depicted in inset in D), and in perituberal neurons. miR147b expression was evident in TSC white matter astrocytes and giant cells whereas in control white matter miR147b was not detected. In TLE-HS hippocampus, increased expression of miR147b was observed in remaining neurons and reactive astrocytes (co-localization with GFAP is depicted in inset in H) within sclerotic areas with gliosis.

miR147b and inflammatory mediators in tuberous sclerosis complex cortical tuber cell cultures

To validate the findings from fetal astrocytes, TSC cell cultures were transfected with miR147b mimic. miR147b overexpression during IL-1β stimulation led to reduced IL-6 and COX-2 mRNA expression levels by approximately 31 and 28%, respectively ($p=0.0022$ and $p<0.0043$ respectively, Fig 6 I-J). There was a trend towards reduced C3 expression after transfection with miR147b mimic ($p=0.0931$, Fig 6K).

Discussion

We aimed to identify which miRNAs are produced by **fetal** human astrocytes during inflammatory conditions *in vitro*, in order to find miRNAs that could be a therapeutic target. We identified miR146a and miR147b to be differentially expressed in **fetal** astrocytes after IL-1β stimulation, which was associated with increased expression of genes related to immune response and inflammation. Overexpression of miR147b reduced the expression of the pro-inflammatory mediators IL-6 and COX-2 after IL-1β stimulation. Transfection of cell cultures with miR146a and miR147b mimics decreased proliferation of **fetal** astrocytes and promoted neuronal differentiation of NSCs. ISH showed increased expression of miR147b in astrocytes in resected brain tissue from patients with TLE-HS and TSC, as compared to controls.

Increased expression of miR146a and miR147b in fetal astrocytes after IL-1β stimulation

Sequencing analysis identified miR146a and miR147b as the two main miRNAs involved in IL-1β mediated inflammation in **fetal** astrocytes. miR146a was previously described in relation to epilepsy and inflammation in astrocytes (Aronica et al. 2010; Gorter et al. 2014; Iyer et al. 2012; van Scheppingen et al. 2016b). miR147b, however, has been described in endothelial cells (Chatterjee et al. 2014), macrophages (Liu et al. 2009) and different types of cancer (Lee et al. 2014; Omrane et al. 2014; Zhang et al. 2016), but has not been described in the epileptogenic brain. mRNA-sequencing identified several GO terms enriched after IL-1β stimulation of **fetal** astrocytes, related to immune response and inflammatory signaling. Correspondingly, the pathway enrichment analysis showed up-regulation of specific pathways related to inflammation like the NF-κB and TNF signaling pathway, confirming the activation of the targeted pathways by IL-1β stimulation. By inhibiting the NF-κB pathway in these cultures using TPCA-1,

an inhibitor of both the IκB kinase-2 (IKK-2), which plays a crucial role NF-κB-regulated production of pro-inflammatory molecules (Podolin et al. 2005), and STAT3, which is also implicated in regulation of IL-6 and COX-2 transcripts (Nan et al. 2014), we confirmed the specific involvement of this pathway in the up-regulation of miR146a and miR147b after stimulation with IL-1β. Finally, mRNA-seq analysis also showed a strong positive correlation between the expression of miR147b and the expression of C15orf48, which is also known as NMES1 (Liu et al. 2009). The pre-miRNA of miR147b is transcribed from a region within the 3' UTR of C15orf48, and since little is known about C15orf48, its strong up-regulation, co-expression and relation to miR147b may warrant further investigation for its role in inflammation.

miR147b mimic acts both under inflammatory and basal conditions on a disintegrin and metalloproteinase15 (ADAM15), which contributes to blood-brain barrier dysfunction and inflammation by increasing vascular permeability and leukocyte migration (Sun et al. 2012). It was previously shown that ADAM15 was targeted by miR147b in human vascular endothelial cells, hereby attenuating albumin passage across endothelial monolayers in vitro (Chatterjee et al. 2014). Thus, the upregulation of miR147b under inflammatory conditions may serve as protective mechanism restoring blood-brain barrier dysfunction. This may be highly beneficial in the epileptogenic brain, as blood-brain barrier dysfunction may contribute to progression of epilepsy (van Vliet et al. 2007).

miR147b overexpression decreased the level of DEPTOR, a mTOR-interacting protein (Peterson et al. 2009), which is activated in both human and experimental epileptogenic brain (Baulac 2016; Citraro et al. 2016; van Vliet et al. 2012). Interestingly, DEPTOR is involved in negative regulation of the mTOR pathway, by inhibiting mTORC1 signaling (Peterson et al. 2009). In the same study, reduction of DEPTOR was also associated with apoptosis and activation of PI3K signaling leading to increased proliferation, however, under our experimental conditions, we did not observe any of these effects. Recent studies suggest also direct inhibitory effects of miR147b on Akt and mTOR activation (Lee et al. 2014; Zhang et al. 2016) that deservers further investigation.

miR147b reduces pro-inflammatory mediators

We found that artificial overexpression of miR147b during inflammatory conditions in **fetal** astrocyte and TSC cell cultures led to decreased expression of pro-inflammatory cytokines IL-6 and COX-2 and complement component 3 (C3). IL-6 and COX-2 have been reported to be associated with astrogliosis in different pathological conditions (Desjardins et al. 2003) and are highly up-regulated in astrocytes after stimulation with IL-1β (Iyer et al. 2012). C3 was recently indicated as one of the most characteristic and highly up-regulated genes in human A1 astrocytes, which are defined as harmful reactive astrocytes that up-regulate classical complement cascade genes and are often found in brain regions associated with disease (Liddelow et al. 2017). Downregulation of C3 might indicate either a decrease in reactivity of the astrocytes or a shift towards the more protective A2 type astrocyte (Liddelow et al. 2017). Thus, miR147b seems to act like a negative regulator of IL-1β induced inflammation, similar to what has been observed for miR146a (van Scheppingen et al. 2016b). In mouse macrophages, it was reported that miR147, the murine homolog for miR147b, was up-regulated after Toll-like receptor 4 (TLR4) activation by LPS, acting as a negative regulator of the macrophage inflammatory response (Liu et al. 2009). In these cultures, miR147b mimic transfection decreased levels of TNF-α and IL-6 under inflammatory conditions, indicating similar functions of this miRNA in various cell types.

miR146a and miR147b decrease proliferation and promote neuronal differentiation

Other than expressing inflammatory cytokines, severe reactive astrogliosis is also associated with other classical hallmarks like increased proliferation and aberrant generation of astrocytes (Sofroniew and Vinters 2010). This is found in the human epileptogenic brain as well as in experimental epilepsy models.

This is illustrated in an astrocyte-specific conditional TSC1 knockout mouse model with spontaneous seizures in which the onset of seizures is concordant with increased astrocytic proliferation (Ortinski et al. 2010; Uhlmann et al. 2002). Also, *in vitro* astrocyte proliferation was found to be increased after treatment with IL-1β (Cui et al. 2011). We found that miR146a and miR147b overexpression decreased the proliferation rate of **fetal** astrocyte cultures. Our results for miR146a are in line with previous studies showing that infection of murine astrocytes with miR146a-overexpressing lentivirus inhibited proliferation (Mei et al. 2011; Nguyen et al. 2016). For miR147b, similar effects are observed in colon cancer cells (Lee et al. 2014) and in a human breast adenocarcinoma cell line, in which overexpression of miR147 led to suppression of proliferation by inhibition of Akt/mTOR signaling (Zhang et al. 2016).

Astrocytes are generated from NSCs, where tight regulation of differentiation is critical for the generation of a balanced number of astrocytes and neurons (Kanski et al. 2014). It was recently reported that neuronal hyperexcitability as seen in epilepsy increases the aberrant generation of astrocytes from NSCs (Sierra et al. 2015). We found that overexpression of miR147b or miR146a induced neuronal differentiation of NSCs derived from fetal brain. Therefore, miR146a and miR147b might have beneficial effects in astrogliosis and scar formation in several pathologies. In order to find targets concerning NSC cell fate decision, we examined multiple targets in two important signaling pathways that instruct astrogenesis: the JAK/STAT pathway and Notch signaling. Inhibition of these pathways would inhibit astrogenesis and promote neurogenesis (Kanski et al. 2014), and indeed, we found targeting of Notch signaling by both miR146a and miR147b, by modulation of NOTCH1. NOTCH1 targeting by miR146a was previously reported in human glioma development and neural stem cell proliferation and differentiation (Mei et al. 2011). miR147b was not predicted to target NOTCH1 by prediction models, however the sequence of miR147b maps on the 3' untranslated region (UTR) of NOTCH1 (miR147b nucleotide 1-7 maps on NOTCH1 nucleotide 52-58, and nucleotide miR147b nucleotide 3-10 maps to NOTCH1 nucleotide 569-562). miR147b also decreased JAK2, hereby also targeting the JAK/STAT pathway. This

could explain why the neuronal fraction is even more increased in differentiated cultures transfected with miR147b mimic.

miR146a and miR147b are expressed in astrocytes in tuberous sclerosis complex and temporal lobe epilepsy

The expression and localization of miR146a has been investigated in our previous studies in TSC (van Scheppingen et al. 2016b), a developmental dysregulation of cortical development, and in TLE-HS (Aronica et al. 2010), in which increased expression of various inflammatory mediators, including IL-1β and gliosis are evident (Vezzani et al. 2011). These studies showed that miR146a was up-regulated in epileptogenic areas where gliosis occurred, and expression was mainly found in reactive astrocytes. We investigated the expression of miR147b in TSC and TLE-HS, and in both pathologies an astrocyte-specific up-regulation of miR147b was observed, confirming the findings in fetal astrocytes after IL-1β stimulation. Expression was also found in giant cells in TSC tubers, which are involved in induction of inflammation in TSC (Boer et al. 2008). Moreover, we cannot exclude that miR147b expression could contribute to the mixed glioneuronal phenotype of these cells. The fact that the expression of miR147 was increased in two different pathologies, both associated with epilepsy, suggests that the occurrence of seizures is a critical factor. However, this needs to be further investigated. Both in control and epileptogenic brain, miR147b was expressed in neurons, indicating possible roles in metabolism, cell growth and synaptic development. Further research would be needed in order to clarify this.

miR147b as possible therapeutic target

Recently, the potential of miR146a to inhibit inflammation in astrocytes was tested *in vivo* (Iori et al. 2017). In this study, miR146a mimic injections in the kainic acid mouse model of TLE inhibited IL-1R1/TLR4 signaling, resulting in arrest of epilepsy progression and an 80% reduction in spontaneous chronic seizures. This is particularly interesting, since this indicates disease modification in epilepsy using a transiently applied miRNA treatment after disease onset. Since miR147b shows a comparable expression pattern in human epileptogenic brain as well as functional effects *in vitro*, and even a more effective modulation of neural stem cell fate decision targeting both NOTCH1 and JAK2, it is worthwhile to investigate the effects of miR147b administration *in vivo* in a similar experimental setup. So far, current antiepileptic drugs provide only symptomatic control of seizures and do not modify epileptogenesis (Weaver and Pohlmann-Eden 2013). Administrating miR147b may be a novel approach to modulate inflammatory pathways underlying epileptogenic pathologies and decrease the generation of reactive astrocytes, hereby targeting mechanisms underlying disease development.

Conclusion

Taken together, using small RNA-sequencing, we found miR147b and miR146a as main miRNAs involved in IL-1β-associated inflammation in **fetal human** astrocyte cultures and both are up-regulated under inflammatory conditions in astrocyte cultures, as well as in the human epileptogenic brain. Since miR147b is capable of providing negative feedback on inflammatory signaling and reducing aberrant proliferation and generation of astrocytes, miR147b deserves further investigation as potential therapeutic agent in neurological disorders associated with inflammation, such as TLE-HS and TSC.

References

Aronica E, Bauer S, Bozzi Y, Caleo M, Dingledine R, Gorter JA, Henshall DC, Kaufer D, Koh S, Loscher W and others. 2017. Neuroinflammatory targets and treatments for epilepsy validated in experimental models. Epilepsia 58 Suppl 3:27-38.

Aronica E, Fluiter K, Iyer A, Zurolo E, Vreijling J, van Vliet EA, Baayen JC, Gorter JA. 2010. Expression pattern of miR-146a, an inflammation-associated microRNA, in experimental and human temporal lobe epilepsy. Eur J Neurosci 31:1100-7.

Aronica E, Ravizza T, Zurolo E, Vezzani A. 2012. Astrocyte immune responses in epilepsy. Glia 60:1258-68.

Baulac S. 2016. mTOR signaling pathway genes in focal epilepsies. Prog Brain Res 226:61-79.

Boer K, Jansen F, Nellist M, Redeker S, van den Ouweland AM, Spliet WG, van Nieuwenhuizen O, Troost D, Crino PB, Aronica E. 2008. Inflammatory processes in cortical tubers and subependymal giant cell tumors of tuberous sclerosis complex. Epilepsy Res 78:7-21.

Bolger AM, Lohse M, Usadel B. 2014. Trimmomatic: a flexible trimmer for Illumina sequence data. Bioinformatics 30:2114-20.

Chatterjee V, Beard RS, Jr., Reynolds JJ, Haines R, Guo M, Rubin M, Guido J, Wu MH, Yuan SY. 2014. MicroRNA-147b regulates vascular endothelial barrier function by targeting ADAM15 expression. PLoS One 9:e110286.

Citraro R, Leo A, Constanti A, Russo E, De Sarro G. 2016. mTOR pathway inhibition as a new therapeutic strategy in epilepsy and epileptogenesis. Pharmacol Res 107:333-43.

Cline MS, Smoot M, Cerami E, Kuchinsky A, Landys N, Workman C, Christmas R, Avila-Campilo I, Creech M, Gross B and others. 2007. Integration of biological networks and gene expression data using Cytoscape. Nat Protoc 2:2366-82.

Colombo E, Farina C. 2016. Astrocytes: Key Regulators of Neuroinflammation. Trends Immunol 37:608-20.

Cui M, Huang Y, Tian C, Zhao Y, Zheng J. 2011. FOXO3a inhibits TNF-α- and IL-1β-induced astrocyte proliferation:Implication for reactive astrogliosis. Glia 59:641-54.

Desjardins P, Sauvageau A, Bouthillier A, Navarro D, Hazell AS, Rose C, Butterworth RF. 2003. Induction of astrocytic cyclooxygenase-2 in epileptic patients with hippocampal sclerosis. Neurochem Int 42:299-303.

Farina C, Aloisi F, Meinl E. 2007. Astrocytes are active players in cerebral innate immunity. Trends Immunol 28:138-45.

Gorter JA, Iyer A, White I, Colzi A, van Vliet EA, Sisodiya S, Aronica E. 2014. Hippocampal subregion-specific microRNA expression during epileptogenesis in experimental temporal lobe epilepsy. Neurobiol Dis 62:508-20.

Huang da W, Sherman BT, Lempicki RA. 2009. Systematic and integrative analysis of large gene lists using DAVID bioinformatics resources. Nat Protoc 4:44-57.

Iori V, Iyer AM, Ravizza T, Beltrame L, Paracchini L, Marchini S, Cerovic M, Hill C, Ferrari M, Zucchetti M and others. 2017. Blockade of the IL-1R1/TLR4 pathway mediates disease-modification therapeutic effects in a model of acquired epilepsy. Neurobiol Dis 99:12-23.

Iyer A, Zurolo E, Prabowo A, Fluiter K, Spliet WG, van Rijen PC, Gorter JA, Aronica E. 2012. MicroRNA-146a: a key regulator of astrocyte-mediated inflammatory response. PLoS One 7:e44789.

Kanski R, van Strien ME, van Tijn P, Hol EM. 2014. A star is born: new insights into the mechanism of astrogenesis. Cell Mol Life Sci 71:433-47.

Lee CG, McCarthy S, Gruidl M, Timme C, Yeatman TJ. 2014. MicroRNA-147 induces a mesenchymal-to-epithelial transition (MET) and reverses EGFR inhibitor resistance. PLoS One 9:e84597.

Li L, Chen XP, Li YJ. 2010. MicroRNA-146a and human disease. Scand J Immunol 71:227-31.

Li MM, Li XM, Zheng XP, Yu JT, Tan L. 2014. MicroRNAs dysregulation in epilepsy. Brain Res 1584:94-104.

Liddelow SA, Guttenplan KA, Clarke LE, Bennett FC, Bohlen CJ, Schirmer L, Bennett ML, Munch AE, Chung WS, Peterson TC and others. 2017. Neurotoxic reactive astrocytes are induced by activated microglia. Nature 541:481-487.

Liu G, Friggeri A, Yang Y, Park Y-J, Tsuruta Y, Abraham E. 2009. miR-147, a microRNA that is induced upon Toll-like receptor stimulation, regulates murine macrophage inflammatory responses. Proceedings of the National Academy of Sciences of the United States of America 106:15819-24.

Mei J, Bachoo R, Zhang CL. 2011. MicroRNA-146a inhibits glioma development by targeting Notch1. Mol Cell Biol 31:3584-92.

Mills JD, Iyer AM, van Scheppingen J, Bongaarts A, Anink JJ, Janssen B, Zimmer TS, Spliet WG, van Rijen PC, Jansen FE and others. 2017. Coding and small non-coding transcriptional landscape of tuberous sclerosis complex cortical tubers: implications for pathophysiology and treatment. Scientific Reports. p ePub ahead of print.

Moynagh PN. 2005. The interleukin-1 signalling pathway in astrocytes: a key contributor to inflammation in the brain. J Anat 207:265-9.

Nan J, Du Y, Chen X, Bai Q, Wang Y, Zhang X, Zhu N, Zhang J, Hou J, Wang Q and others. 2014. TPCA-1 is a direct dual inhibitor of STAT3 and NF-kappaB and regresses mutant EGFR-associated human non-small cell lung cancers. Mol Cancer Ther 13:617-29.

Nguyen LS, Lepleux M, Makhlouf M, Martin C, Fregeac J, Siquier-Pernet K, Philippe A, Feron F, Gepner B, Rougeulle C and others. 2016. Profiling olfactory stem cells from living patients identifies miRNAs relevant for autism pathophysiology. Mol Autism 7:1.

Omrane I, Kourda N, Stambouli N, Privat M, Medimegh I, Arfaoui A, Uhrhammer N, Bougatef K, Baroudi O, Bouzaienne H and others. 2014. MicroRNAs 146a and 147b biomarkers for colorectal tumor's localization. Biomed Res Int 2014:584852.

Ortinski PI, Dong J, Mungenast A, Yue C, Takano H, Watson DJ, Haydon PG, Coulter DA. 2010. Selective induction of astrocytic gliosis generates deficits in neuronal inhibition. Nat Neurosci 13:584-91.

Peterson TR, Laplante M, Thoreen CC, Sancak Y, Kang SA, Kuehl WM, Gray NS, Sabatini DM. 2009. DEPTOR is an mTOR inhibitor frequently overexpressed in multiple myeloma cells and required for their survival. Cell 137:873-86.

Podolin PL, Callahan JF, Bolognese BJ, Li YH, Carlson K, Davis TG, Mellor GW, Evans C, Roshak AK. 2005. Attenuation of murine collagen-induced arthritis by a novel, potent, selective small molecule inhibitor of IkappaB Kinase 2, TPCA-1 (2-[(aminocarbonyl)amino]-5-(4-fluorophenyl)-3-thiophenecarboxamide), occurs via reduction of proinflammatory cytokines and antigen-induced T cell Proliferation. J Pharmacol Exp Ther 312:373-81.

Ravizza T, Gagliardi B, Noe F, Boer K, Aronica E, Vezzani A. 2008. Innate and adaptive immunity during epileptogenesis and spontaneous seizures: evidence from experimental models and human temporal lobe epilepsy. Neurobiol Dis 29:142-60.

Sierra A, Martin-Suarez S, Valcarcel-Martin R, Pascual-Brazo J, Aelvoet SA, Abiega O, Deudero JJ, Brewster AL, Bernales I, Anderson AE and others. 2015. Neuronal hyperactivity accelerates depletion of neural stem cells and impairs hippocampal neurogenesis. Cell Stem Cell 16:488-503.

Sofroniew MV, Vinters HV. 2010. Astrocytes: biology and pathology. Acta Neuropathol 119:7-35.

Sparacio SM, Zhang Y, Vilcek J, Benveniste EN. 1992. Cytokine regulation of interleukin-6 gene expression in astrocytes involves activation of an NF-kappa B-like nuclear protein. J Neuroimmunol 39:231-42.

Srinivasan D, Yen JH, Joseph DJ, Friedman W. 2004. Cell type-specific interleukin-1beta signaling in the CNS. J Neurosci 24:6482-8.

Sun C, Wu MH, Lee ES, Yuan SY. 2012. A disintegrin and metalloproteinase 15 contributes to atherosclerosis by mediating endothelial barrier dysfunction via Src family kinase activity. Arterioscler Thromb Vasc Biol 32:2444-51.

Uhlmann EJ, Wong M, Baldwin RL, Bajenaru ML, Onda H, Kwiatkowski DJ, Yamada K, Gutmann DH. 2002. Astrocyte-specific TSC1 conditional knockout mice exhibit abnormal neuronal organization and seizures. Ann Neurol 52:285-96.

van Scheppingen J, Broekaart DW, Scholl T, Zuidberg MR, Anink JJ, Spliet WG, van Rijen PC, Czech T, Hainfellner JA, Feucht M and others. 2016a. Dysregulation of the (immuno)proteasome pathway in malformations of cortical development. J Neuroinflammation 13:202.

van Scheppingen J, Iyer AM, Prabowo AS, Mühlebner A, Anink JJ, Scholl T, Feucht M, Jansen FE, Spliet WG, Krsek P and others. 2016b. Expression of microRNAs miR21, miR146a, and miR155 in tuberous sclerosis complex cortical tubers and their regulation in human astrocytes and SEGA-derived cell cultures. Glia 64:1066-82.

van Vliet EA, da Costa Araujo S, Redeker S, van Schaik R, Aronica E, Gorter JA. 2007. Blood-brain barrier leakage may lead to progression of temporal lobe epilepsy. Brain 130:521-34.

van Vliet EA, Forte G, Holtman L, den Burger JC, Sinjewel A, de Vries HE, Aronica E, Gorter JA. 2012. Inhibition of mammalian target of rapamycin reduces epileptogenesis and blood-brain barrier leakage but not microglia activation. Epilepsia 53:1254-63.

Vezzani A, French J, Bartfai T, Baram TZ. 2011. The role of inflammation in epilepsy. Nat Rev Neurol 7:31-40.

Weaver DF, Pohlmann-Eden B. 2013. Pharmacoresistant epilepsy: unmet needs in solving the puzzle(s). Epilepsia 54 Suppl 2:80-5.

Xanthos DN, Sandkuhler J. 2014. Neurogenic neuroinflammation: inflammatory CNS reactions in response to neuronal activity. Nat Rev Neurosci 15:43-53.

Zhang Y, Zhang HE, Liu Z. 2016. MicroRNA-147 suppresses proliferation, invasion and migration through the AKT/mTOR signaling pathway in breast cancer. Oncol Lett 11:405-410.

Figure legends

FIGURE 1: Differentially expressed small RNAs and mRNAs as identified from RNA-Seq. **A** Volcano plot of differentially expressed small RNAs as identified from small RNA-Seq. Across both the controls and IL-1β stimulated **fetal human astrocyte** cultures there were 881 expressed small RNAs. Of these only miR146a-5p and miR147b were differentially expressed. miR147b was up-regulated 3.78-fold in the IL-1β stimulated cultures (adjusted p-value<0.033), while miR146a-5p was up-regulated 5.35-fold in the IL-1β stimulated cultures (adjusted p-value<0.0008). **B** Volcano plot of differentially expressed mRNAs as identified from mRNA-Seq. Volcano plot showing the differential expressed genes between the control cultures and IL-1β stimulated cultures. 71 genes were up-regulated in the IL-1β stimulated cultures (adjusted p-value<0.05, fold-change>2), and 8 genes were down-regulated (adjusted p-value<0.05, fold-change<-2). **C** Enriched gene ontology terms derived from the differentially expressed gene lists. 16 GO terms were identified as enriched (Benjamini-Hochberg corrected p-value<0.05). Each enriched GO term is listed on the y-axis, the x-axis is the log10(1/adjusted p-value), n is equal to the number of the DEGs in each gene ontology terms. **D** Enrichment map of enriched pathways derived from the differentially expressed gene lists. 12 pathways were considered enriched (Benjamini-Hochberg corrected p-value<0.05). Each node represents a pathway, the size of the node reflects the statistical significance of each pathway. The larger the node the smaller the adjusted p-value e.g. TNF signaling pathway was statistically more significant than the retinoic acid-inducible gene I (RIG-I)-like receptor signaling pathway. The edge connection between nodes represents the similarity between the genes list of each pathway, the thicker the edge the more similar the gene lists.

FIGURE 2: miR147b decreases inflammation in astrocytes. Quantitative real-time PCR of miRNA or mRNA expression (**A-C, E**) and ELISA analysis of protein levels (**D**) in **fetal** human astrocyte cultures. **A** Astrocytes were treated with IL-1β (10 ng/ml) or LPS (100 ng/ml) for 1, 6, 24, 30 and 48 hours. miR147b was up-regulated after stimulation with IL-1β with peak expression at 30 hours. **B** TPCA-1 decreased both miR146a and miR147b expression. **C-E** Astrocytes were transfected for 24 hours with miR147b mimic (50 nM) followed by 24 hours of IL-1β stimulation. miR147b mimic decreased the mRNA levels of pro-inflammatory markers IL-6 and COX-2 and reactivity marker C3 (**C**), and the level of IL-6 in culture supernatants (**D**). **E** miR147b mimic decreased the mRNA levels of predicted targets DEPTOR and ADAM15. Experiments were performed in triplicate and data are mean ± SEM. *p<0.05, **p<0.01, ***p<0.001 compared to control, Kruskall-Wallis with Dunn's post-hoc test (**A**) and Mann Whitney U test (**B-E**).

FIGURE 3: Proliferation of astrocytes after transfection with miR146a and miR147b mimics. **Fetal** human astrocytes were transfected for 24 hours with miRNA mimic (50 nM) and after a total of three days stained with anti-Ki67 antibody (**A** and **B**) or propidium iodine (PI, **C**). **A** Representative Ki67 staining in control cells and cells treated with miR146a or miR147b mimic. **B** Quantification of Ki67 staining showed decreased proliferation after miR146a and miR147b mimic transfection compared to control. **C** Both miR146a and miR147b mimic transfected cells showed lesser cells in the S-phase compared to control cells. Data are expressed relative to the levels observed in cells treated with transfection reagent only and are mean ± SEM of two experiments from two donors performed in triplicate. Cells in **A** were counterstained with phalloidin (actin filaments; red) and diamidino-2-phenylindole, DAPI (nuclei; blue). Scale bar in **A**: 50 µM. *p<0.05, **p<0.01 compared to control, Mann Whitney U test.

FIGURE 4: Culturing and differentiation of fetal neural stem cells (NSCs). Phase contrast pictures of live cells in culture and confocal images of fixed and immunostained cells. **A** and **B** NSCs were grown in **floating conditions where they formed clusters of cells** (**A**) and secondary cultures could be formed after dissociation and re-plating (**B**). **C** NSCs expressed stem cell markers Nestin and SOX2. **D-G** Expression of GFAP and βIII-tubulin was low in NSCs. **H-O** After differentiation with 5% FCS for 7 or 14 days, strong immunoreactivity for βIII-tubulin and GFAP was visible. Scale bar in **B**: 100 µm (**A**-**B**); scale bar in **C**, **N**, **O**: 50 µm (**C**-**O**).

FIGURE 5: Differentiation of fetal neural stem cells (NSCs) after transfection with miR146a and miR147b **mimics**. NSCs were transfected with miRNA mimic (50 nM) for 24 hours, followed by 7 days of differentiation. **A-L** Confocal images of fixed and immunostained cells and phase contrast pictures of live cells in culture. Cells were stained for βIII-tubulin, GFAP and counterstained with DAPI. The βIII-tubulin-positive cells and DAPI nuclei were quantified. **M** The βIII-tubulin/DAPI ratio was increased after transfection with miR146a or miR147b mimics. **N** and **O** Quantitative real-time PCR of target mRNA expression in NSC cultures 48 hours after initiation of differentiation. **N** NOTCH1 expression was decreased after transfection with miR146a or miR147b mimics. **O** miR147b **mimic** decreased the expression of JAK2. Scale bar in **K** and **L**: 50 μM. Experiments in **I**-**K** were performed in triplicate in cultures from three separate donors and data are mean ± SEM. *p<0.05, **p<0.01 compared to control, Mann Whitney U test.

FIGURE 6: miR147b expression in tuberous sclerosis complex (TSC) cortical tubers and temporal lobe epilepsy with hippocampal sclerosis (TLE-HS), and modulation of inflammation by miR147b in TSC cortical tuber cell cultures. **A**-**H** In situ hybridization of miR147b expression in TSC, TLE-HS and control brain tissue. In control cortex, miR147b expression is only visible in neurons in the gray matter (GM, arrows in **A**), with no expression in the white matter (WM, **C**). In TSC tubers, besides expression in dysmorphic neurons and giant cells (arrows in **B** and **D**), miR147b is also visible in astrocytes (arrow heads, **B** and **D**). Inset in **D** shows co-localization of miR147b with GFAP in the tuber. In control hippocampus, miR147b is expressed by neurons (**E**, **G**), whereas in TLE-HS expression is also localized in astrocytes (arrowheads in **F** and **H**) besides neurons (arrows in **F** and **H**). Inset in **H** shows co-localization of miR147b with GFAP in the hilus. **I-K** Quantitative real-time PCR of mRNA expression in TSC cell cultures. TSC cells were transfected for 24 hours with miR147b mimic (50 nM) followed by 24 hours of IL-1β stimulation (10 ng/ml). miR147b mimic decreased the mRNA levels of pro-inflammatory cytokines IL-6 (**I**) and COX-2 (**J**), complement component 3 (C3) showed a trend towards decreased expression (**K**). Scale bar in **H**: 100 μm, in inset: 25 μm. ***$p<0.001$ compared to control, Mann Whitney U test. Experiments in **I**-**K** were performed in triplicate in cultures from two separate donors and data are mean ± SEM. **$p<0.01$, Mann Whitney U test.

TABLE 1: Enriched gene ontology (GO) terms and associated differential expressed mRNAs as determined by mRNA-sequencing of control and IL-1β stimulated human astrocyte cultures.

Gene ontology category	Term ID	Gene ontology term	Gene count	Genes
Biological Process	GO:0060337	type I interferon signaling pathway	9	IRF1, IFI6, OAS2, OAS3, IFI35, MX1, ISG15, GBP2, OAS1
Biological Process	GO:0051607	defense response to virus	10	IRF1, PLSCR1, OAS2, IFI44L, DDX60, OAS3, MX1, ISG15, IL6, OAS1
Biological Process	GO:0006954	inflammatory response	13	CCL20, C3, PLA2G4C, NFKBIZ, TNIP1, RELB, CSF1, PTX3, IL6, NFKB2, CXCL8, TNFAIP6, TNFAIP3
Biological Process	GO:0006955	immune response	13	IL32, CCL20, IFI6, OAS2, LIF, OAS3, C1R, IL6, GBP2, CXCL8, C3, IL7R, OAS1
Biological Process	GO:0045071	negative regulation of viral genome replication	6	TNIP1, PLSCR1, OAS3, MX1ISG15, OAS1
Biological Process	GO:0009615	response to virus	7	OAS2, DDX60, IFI44, OAS3, MX1, IFIH1, OAS1
Biological Process	GO:0060333	interferon-gamma-mediated signaling pathway	6	IRF1, OAS2, OAS3, VCAM1, GBP2, OAS1
Biological Process	GO:0032480	negative regulation of type I interferon production	4	UBE2L6, IFIH1, ISG15, TNFAIP3
Biological Process	GO:0045087	innate immune response	9	DDX60, RELB, CSF1, C1R, APOL1, MX1, IFIH1, NFKB2, PTX3
Biological Process	GO:0045944	positive regulation of transcription from RNA polymerase II promoter	13	NFKBIA, IRF1, POU2F2, HELZ2, TNIP1, PARK2, PLSCR1, LIF, IL11, RELB, NAMPT, NFKB2, IL6
Biological Process	GO:0046888	negative regulation of hormone secretion	3	LIF, IL11, IL6
Cellular Compart-ment	GO:0005615	extracellular space	21	IL32, AKR1B1, CCL20, LIF, IL11, CHI3L2, OAS3, NAMPT, ABI3BP, C1QTNF1, C3, PAPPA, TNFAIP2, VCAM1, CSF1, APOL1, STC1, IL6, PTX3, CXCL8, TNFAIP6
Cellular Compart-ment	GO:0005829	cytosol	25	NFKBIA, AKR1B1, IL32, PLSCR1, UBE2L6, PARK2, OAS2, OAS3, AMPD3, NAMPT, ISG15, GBP2, OAS1, IRF1, PLA2G4C, HERC6, BIRC3, IFI35, FHIT, GRIP1, RELB, MX1, IFIH1, NFKB2, TNFAIP3
Molecular Function	GO:0001730	2'-5'-oligoadenylate synthetase activity	3	OAS2, OAS3, OAS1
Molecular Function	GO:0003725	double-stranded RNA binding	5	OAS2, DDX60, OAS3, IFIH1, OAS1
Molecular Function	GO:0005125	cytokine activity	6	IL32, LIF, CSF1, NAMPT, IL6

TABLE 2: Enriched pathway terms and associated differential expressed mRNAs as determined by mRNA-sequencing of control and IL-1β stimulated human astrocyte cultures.

Pathway	Gene count	Genes	P value	Adjusted p-value[a]
hsa04668: TNF signaling pathway	8	NFKBIA, BIRC3, CCL20, LIF, CSF1, VCAM1, IL6, TNFAIP3	7.74E-07	7.97E-05
hsa04064: NF-kappa B signaling pathway	7	NFKBIA, BIRC3, RELB, VCAM1, NFKB2, CXCL8, TNFAIP3	4.05E-06	1.39E-04
hsa05162: Measles	8	NFKBIA, OAS2, OAS3, MX1, IFIH1, IL6, TNFAIP3, OAS1	3.58E-06	1.85E-04
hsa05164: Influenza A	8	NFKBIA, OAS2, OAS3, MX1, IFIH1, IL6, CXCL8, OAS1	2.11E-05	5.43E-04
hsa05160: Hepatitis C	7	NFKBIA, IRF1, OAS2, OAS3, CLDN1, CXCL8, OAS1	4.66E-05	9.59E-04
hsa04621: NOD-like receptor signaling pathway	5	NFKBIA, BIRC3, IL6, CXCL8, TNFAIP3	1.57E-04	0.00230227
hsa05134: Legionellosis	5	NFKBIA, NFKB2, IL6, CXCL8, C3	1.46E-04	0.00249934
hsa05168: Herpes simplex infection	7	NFKBIA, OAS2, OAS3, IFIH1, IL6, C3, OAS1	2.72E-04	0.00349796
hsa05133: Pertussis	5	IRF1, C1R, IL6, CXCL8, C3	5.20E-04	0.00592968
hsa05323: Rheumatoid arthritis	5	CCL20, IL11, CSF1, IL6, CXCL8	9.51E-04	0.00887256
hsa04060: Cytokine-cytokine receptor interaction	7	CCL20, LIF, CSF1, IL6, CSCL8, IL7R	9.20E-04	0.00943084
hsa04622: RIG-I-like receptor signaling pathway	4	NFKBIA, IFIH1, ISG15, CXCL8	0.00516713	0.04349202

[a]Benjamini-Hochberg adjusted p-value.

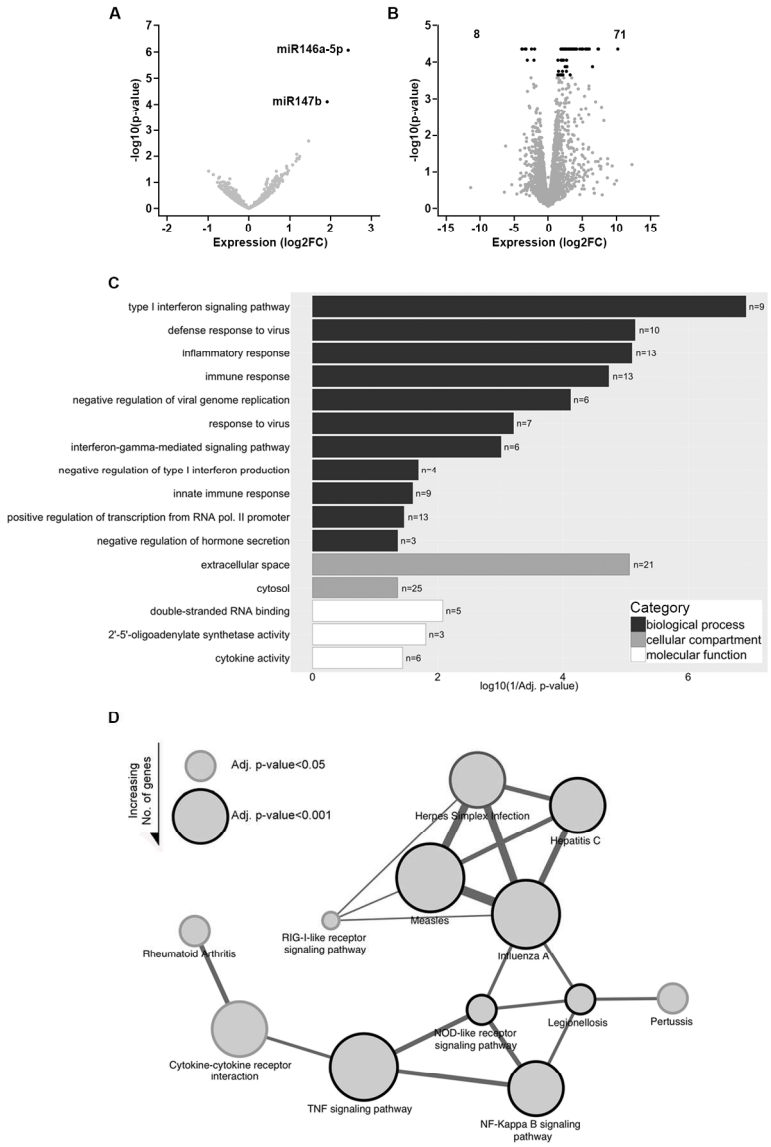

FIGURE 1: Differentially expressed small RNAs an mRNAs as identified from RNA-Seq. A Volcano plot of differentially expressed small RNAs as identified from small RNA-Seq. Across both the controls and IL-1β stimulated cultures there were 881 expressed small RNAs. Of these only miR146a-5p and miR147b were differentially expressed. miR147b was up-regulated 3.78-fold in the IL-1β stimulated cultures (adjusted p-value<0.033), while miR146a-5p was up-regulated 5.35-fold in the IL-1β stimulated cultures (adjusted p-value<0.0008). B Volcano plot of differentially expressed mRNAs as identified from mRNA-Seq. Volcano plot showing the differential expressed genes between the control cultures and IL-1β stimulated cultures. 71 genes were up-regulated in the IL-1β stimulated cultures (adjusted p-value<0.05, fold-change>2), and 8 genes were down-regulated (adjusted p-value<0.05, fold-change<-2). C Enriched gene ontology terms derived from the differentially expressed gene lists. 16 GO terms were identified as enriched (Benjamini-Hochberg corrected p-value<0.05). Each enriched GO term is listed on the y-axis, the x-axis is the log10(1/adjusted p-value), n is equal to the number of the DEGs in each gene ontology terms. D Enrichment map of enriched pathways derived from the differentially expressed gene lists. 12 pathways were considered

enriched (Benjamini-Hochberg corrected p-value<0.05). Each node represents a pathway, the size of the node reflects the statistical significance of each pathway. The larger the node the smaller the adjusted p-value e.g. TNF signaling pathway was statistically more significant than the retinoic acid-inducible gene I (RIG-I)-like receptor signaling pathway. The edge connection between nodes represents the similarity between the genes list of each pathway, the thicker the edge the more similar the gene lists.

170x235mm (300 x 300 DPI)

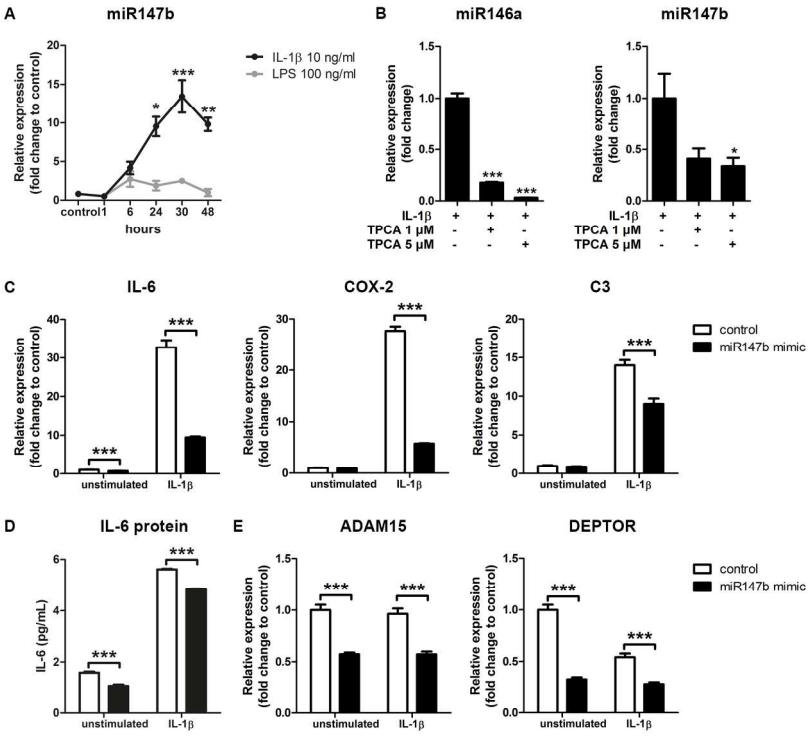

FIGURE 2: miR147b decreases inflammation in astrocytes. Quantitative real-time PCR of miRNA or mRNA expression (A-C, E) and ELISA analysis of protein levels (D) in human astrocyte cultures. A Astrocytes were treated with IL-1β (10 ng/ml) or LPS (100 ng/ml) for 1, 6, 24, 30 and 48 hours. miR147b was up-regulated after stimulation with IL-1β with peak expression at 30 hours. B TPCA-1 decreased both miR146a and miR147b expression. C-E Astrocytes were transfected for 24 hours with miR147b mimic (50 nM) followed by 24 hours of IL-1β stimulation. miR147b mimic decreased the mRNA levels of pro-inflammatory markers IL-6 and COX-2 and reactivity marker C3 (C), and the level of IL-6 in culture supernatants (D). E miR147b mimic decreased the mRNA levels of predicted targets DEPTOR and ADAM15. Experiments were performed in triplicate and data are mean ± SEM. *p<0.05, **p<0.01, ***p<0.001 compared to control, Kruskall-Wallis with Dunn's post-hoc test (A) and Mann Whitney U test (B-E).

170x235mm (300 x 300 DPI)

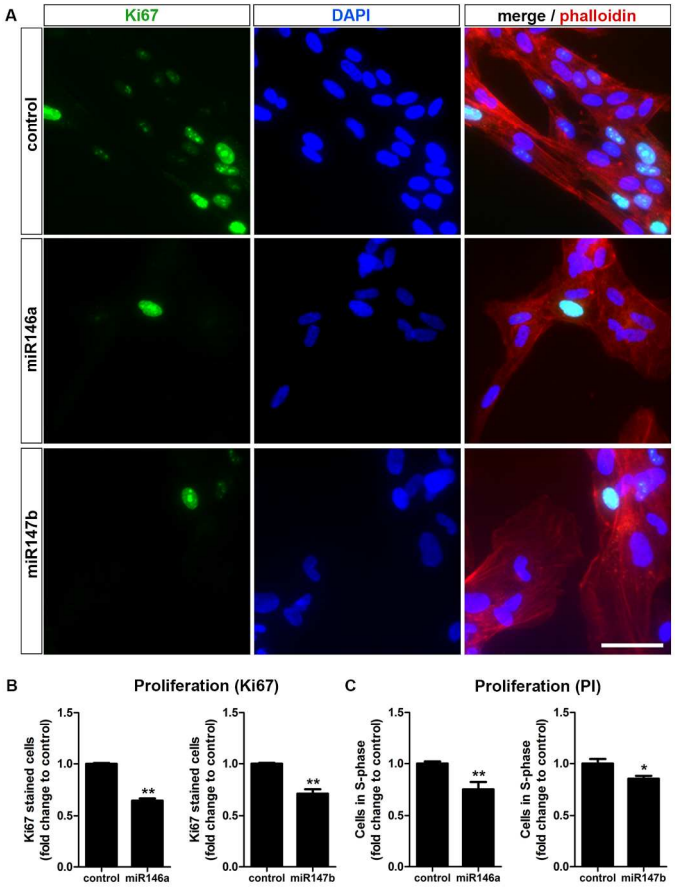

FIGURE 3: Proliferation of fetal astrocytes after transfection with miR146a and miR147b mimics. Astrocytes were transfected for 24 hours with miRNA mimic (50 nM) and after a total of three days stained with anti-Ki67 antibody (A and B) or propidium iodine (PI, C). A Representative Ki67 staining in control cells and cells treated with miR146a or miR147b mimic. B Quantification of Ki67 staining showed decreased proliferation after miR146a and miR147b mimic transfection compared to control. C Both miR146a and miR147b mimic transfected cells showed lesser cells in the S-phase compared to control cells. Data are expressed relative to the levels observed in cells treated with transfection reagent only and are mean ± SEM of two experiments from two donors performed in triplicate. Cells in A were counterstained with phalloidin (actin filaments; red) and diamidino-2-phenylindole, DAPI (nuclei; blue). Scale bar in A: 50 µM. *p<0.05, **p<0.01 compared to control, Mann Whitney U test.

170x235mm (300 x 300 DPI)

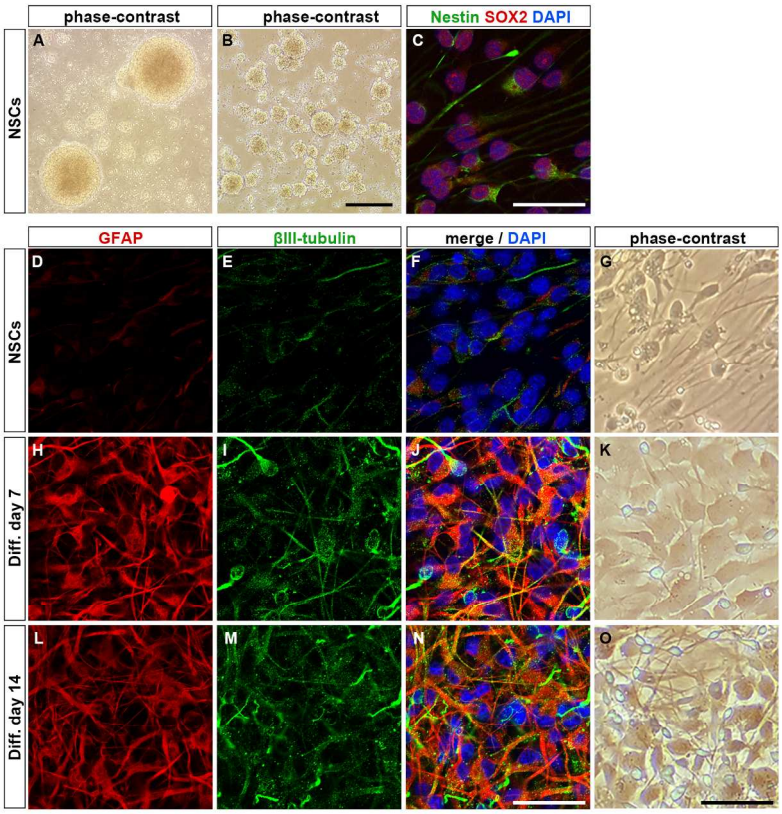

FIGURE 4: Culturing and differentiation of fetal neural stem cells (NSCs). Phase contrast pictures of live cells in culture and confocal images of fixed and immunostained cells. A and B NSCs were grown in floating conditions where they formed clusters of cells (A) and secondary cultures could be formed after dissociation and re-plating (B). C NSCs expressed stem cell markers Nestin and SOX2. D-G Expression of GFAP and βIII-tubulin was low in NSCs. H-O After differentiation with 5% FCS for 7 or 14 days, strong immunoreactivity for βIII-tubulin and GFAP was visible. Scale bar in B: 100 µm (A-B); scale bar in C, N, O: 50 µm (C-O).

170x235mm (300 x 300 DPI)

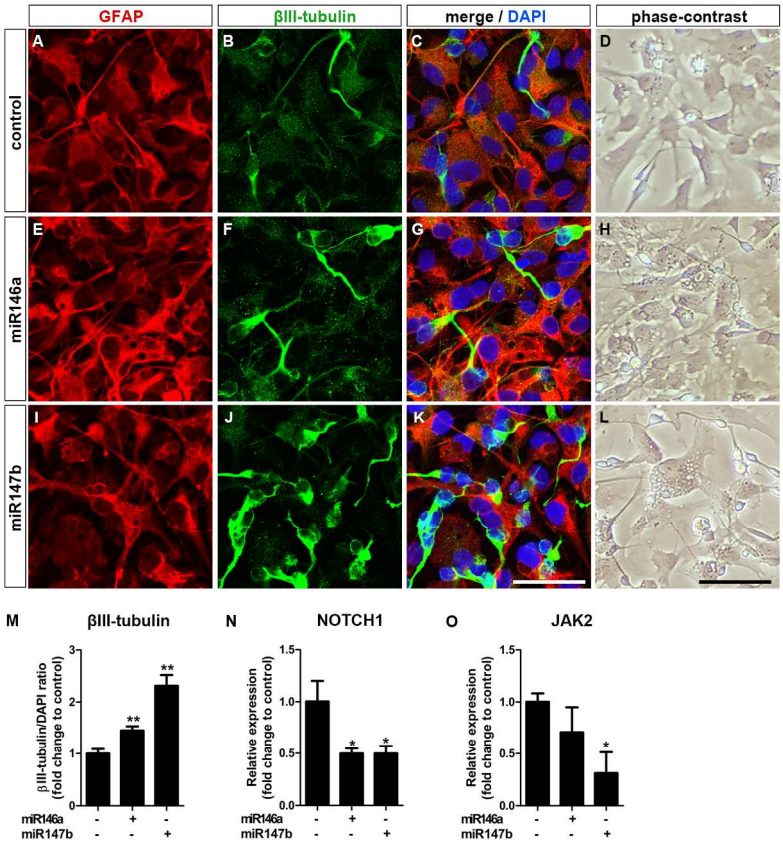

FIGURE 5: Differentiation of fetal neural stem cells (NSCs) after transfection with miR146a and miR147b mimics. NSCs were transfected with miRNA mimic (50 nM) for 24 hours, followed by 7 days of differentiation. A-L Confocal images of fixed and immunostained cells and phase contrast pictures of live cells in culture. Cells were stained for βIII-tubulin, GFAP and counterstained with DAPI. The βIII-tubulin-positive cells and DAPI nuclei were quantified. M The βIII-tubulin/DAPI ratio was increased after transfection with miR146a or miR147b mimics. N and O Quantitative real-time PCR of target mRNA expression in NSC cultures 48 hours after initiation of differentiation. N NOTCH1 expression was decreased after transfection with miR146a or miR147b mimics. O miR147b mimic decreased the expression of JAK2. Scale bar in K and L: 50 μM. Experiments in I-K were performed in triplicate in cultures from three separate donors and data are mean ± SEM. *p<0.05, **p<0.01 compared to control, Mann Whitney U test.

180x235mm (300 x 300 DPI)

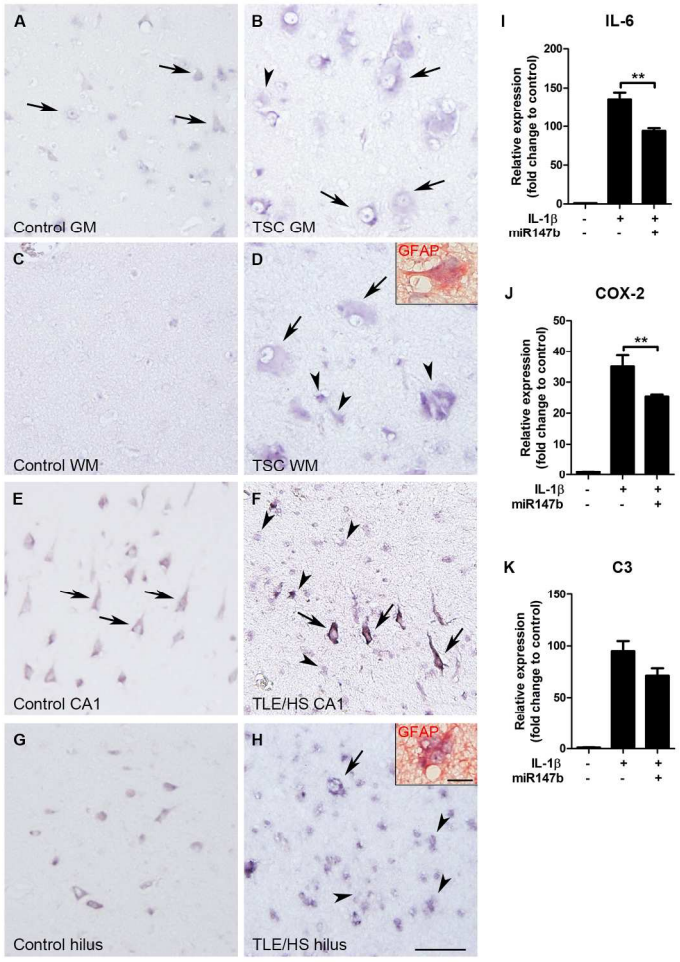

FIGURE 6: miR147b expression in tuberous sclerosis complex (TSC) cortical tubers and temporal lobe epilepsy with hippocampal sclerosis (TLE-HS), and modulation of inflammation by miR147b in TSC cortical tuber cell cultures. A-H In situ hybridization of miR147b expression in TSC, TLE-HS and control brain tissue. In control cortex, miR147b expression is only visible in neurons in the gray matter (GM, arrows in A), with no expression in the white matter (WM, C). In TSC tubers, besides expression in dysmorphic neurons and giant cells (arrows in B and D), miR147b is also visible in astrocytes (arrow heads, B and D). Inset in D shows co-localization of miR147b with GFAP in the tuber. In control hippocampus, miR147b is expressed by neurons (E, G), whereas in TLE-HS expression is also localized in astrocytes (arrowheads in F and H) besides neurons (arrows in F and H). Inset in H shows co-localization of miR147b with GFAP in the hilus. I-K Quantitative real-time PCR of mRNA expression in TSC cell cultures. TSC cells were transfected for 24 hours with miR147b mimic (50 nM) followed by 24 hours of IL-1β stimulation (10 ng/ml). miR147b mimic decreased the mRNA levels of pro-inflammatory cytokines IL-6 (I) and COX-2 (J), complement component 3 (C3) showed a trend towards decreased expression (K). Scale bar in H: 100 μm, in inset: 25 μm.

***p<0.001 compared to control, Mann Whitney U test. Experiments in I-K were performed in triplicate in cultures from two separate donors and data are mean ± SEM. **p<0.01, Mann Whitney U test.

170x235mm (300 x 300 DPI)

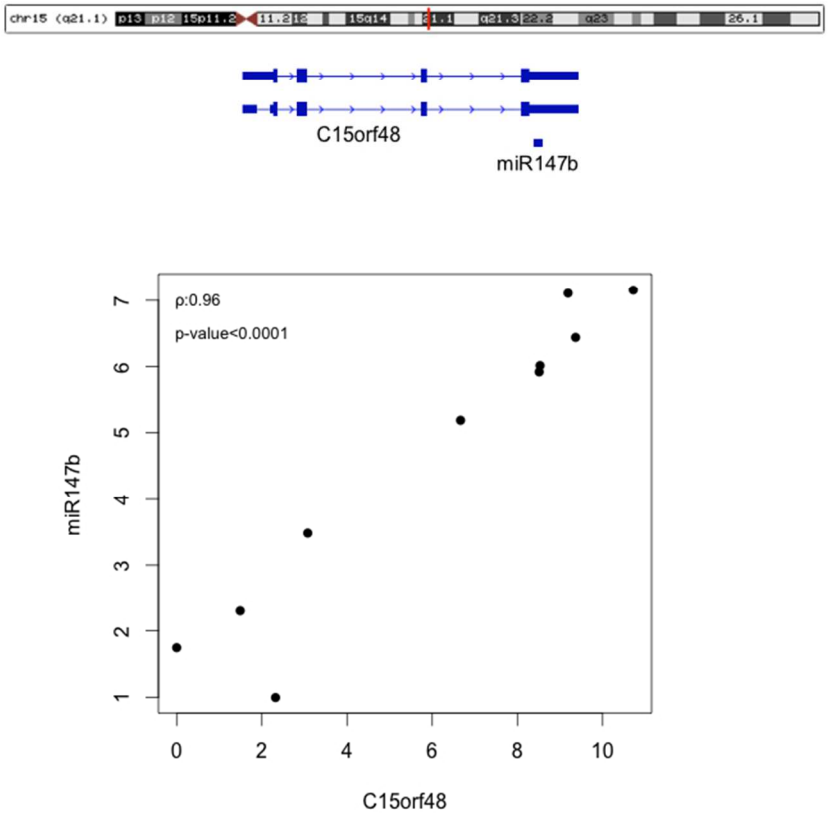

SUPPLEMENTARY FIGURE 1: Relationship between C15orf48 and miR147b. The genomic location of C15orf48 and miR147b is shown. Both transcripts are transcribed from the same template strand on chromosome 15. The pre-miR147b transcript is harbored within a region that is also transcribed as the 3' UTR of C15orf48. There was a strong correlation between miR147b and C15orf48 expression levels (ρ=0.96, p-value<0.0001, Spearman's rank correlation test). Expression is shown in log2(normalized read-counts+1).

275x258mm (72 x 72 DPI)

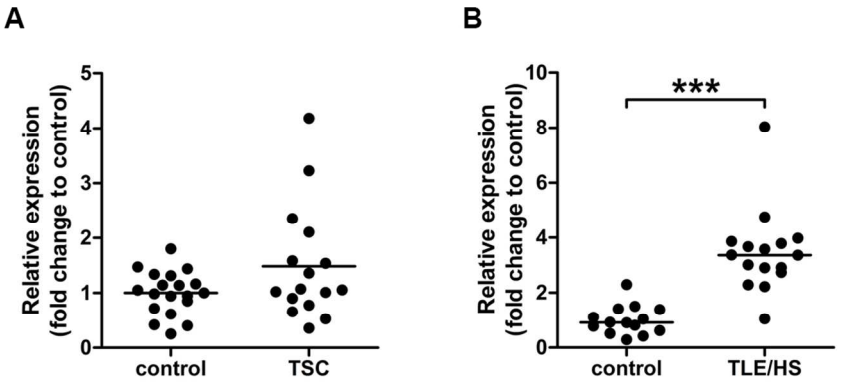

SUPPLEMENTARY FIGURE 2: miR147b expression in tuberous sclerosis complex (TSC) cortical tubers and temporal lobe epilepsy with hippocampal sclerosis (TLE-HS). Quantitative real-time PCR of fresh frozen brain tissue. A miR147b expression levels in TSC tubers (n=16) did not differ to expression in control cortex (n=19), however increased levels are observed in a subset of patients. B expression levels in TLE-HS (n=16) were increased compared to control hippocampus (n=14).

109x60mm (300 x 300 DPI)

Supplementary Table 1 Primer sequences.

	Forward primer (5'-3')	Reverse primer (5'-3')
IL-6	ctcagccctgagaaaggaga	tttcagccatctttggaagg
COX-2	gaatggggtgatgagcagtt	gccactcaagtgttgcacat
DEPTOR	tgagaggacagaggctatatgaaa	tgaaggtgcgctcatacttg
ADAM15	ggcatggccattcagaac	aggatgctggtggagtggt
IL-32	ctctgtctctctcggctgagtat	cggccaaaagttcaagga
EF1A	atccacctttgggtcgcttt	ccgcaactgtctgtctcatatcac
C1orf43	gatttccctgggtttccagt	attcgactctccagggttca
NOTCH1	ctgcctgtctgaggtcaatg	tcacagtcgcacttgtaccc
JAK2	caaaaaccaggcgctgaact	tgccactgcaataccaacga
C3	cctgaagatagagggtgacca	ccaccacgtcccagatctta

Supplementary Table 2 Complete list of differentially expressed mRNAs as determined by mRNA-sequencing of control and IL-1β stimulated human astrocyte cultures.

Gene	Description	Location	Control FPKM	IL-1β FPKM	Log2(Fold Change)	p-value	Adjusted p-value[a]
CCL20	C-C motif chemokine ligand 20	chr2:227813841-227817564	0	51.2757	inf	5.00E-05	0.0124559
OAS2	2'-5'-oligoadenylate synthetase 2	chr12:112906776-113017751	0.146736	13.1993	6.4911	0.00015	0.0310521
OAS1	2'-5'-oligoadenylate synthetase 1	chr12:112906776-113017751	0.153149	25.2314	7.36414	5.00E-05	0.0124559
FCRLA	Fc receptor like A	chr1:161706971-161714352	0.309749	1.20955	1.9653	0.00025	0.0453642
C3	complement C3	chr19:6677703-6737603	0.310427	20.0424	6.01266	5.00E-05	0.0124559
APOL1	apolipoprotein L1	chr22:36253009-36267530	0.384288	3.53226	3.20033	5.00E-05	0.0124559
MCTP1	multiple C2 and transmembrane domain containing 1	chr5:941529655-95284575	0.418875	1.89586	2.17826	5.00E-05	0.0124559
LUCAT1	lung cancer associated transcript 1 (non-protein coding)	chr5:91302030-91314484	0.602348	6.1486	3.35159	5.00E-05	0.0124559
IFI44L	interferon induced protein 44 like	chr1:78619921-78647788	0.798437	44.5501	5.80211	5.00E-05	0.0124559
BIRC3	baculoviral IAP repeat containing 3	chr11:102317449-102339403	0.881077	21.8314	4.63099	5.00E-05	0.0124559
HERC6	HECT and RLD domain containing E3 ubiquitin protein ligase family member 6	chr4:883786988443111	0.948065	14.3077	3.91566	5.00E-05	0.0124559
IFIH1	interferon induced with helicase C domain 1	chr2:162267078-162318703	1.08361	10.076	3.21699	0.00025	0.0453642
SLC7A2	solute carrier family 7 member 2	chr8:174943677570573	1.1903	39.438	5.05018	5.00E-05	0.0124559
MX1	MX dynamin like GTPase 1	chr21:41420303-41459214	1.20825	53.308	5.46336	5.00E-05	0.0124559
IL6	interleukin 6	chr7:22725394-22732002	1.50528	236.633	7.29648	5.00E-05	0.0124559
OAS3	2'-5'-oligoadenylate synthetase 3	chr12:112906776-113017751	1.54914	27.6823	4.15943	5.00E-05	0.0124559
RAB27B	RAB27B, member RAS oncogene family	chr18:54717859-54898083	1.61661	7.16462	2.14792	0.00025	0.0453642
CHI3L2	chitinase 3 like 2	chr1:111186326-111243440	1.63045	19.0502	3.54646	5.00E-05	0.0124559
DDX60	DExD/H-box helicase 60	chr4:168216292-168318807	1.70224	9.23533	2.43973	5.00E-05	0.0124559
TNFAIP2	TNF alpha induced protein 2	chr14:103123441-103137440	1.73929	85.6917	5.62258	5.00E-05	0.0124559
CXCL8	C-X-C motif chemokine ligand 8	chr4:737405073743716	2.03126	2393.87	10.2028	5.00E-05	0.0124559
HELZ2	helicase with zinc finger 2	chr20:63558085-63574239	2.05428	8.68881	2.08053	0.0002	0.0397243

PLA2G4C	phospholipase A2 group IVC	chr19:48047842-48110824	2.11715	5.64599	1.4151	0.0001	0.0219373
C1QTNF1	C1q and tumor necrosis factor related protein 1	chr17:79019208-79049788	2.2431	68.3922	4.93026	5.00E-05	0.0124559
POU2F2	POU class 2 homeobox 2	chr19:42086107-42196585	2.26248	14.6095	2.69093	0.0001	0.0219373
RRAD	RRAD, Ras related glycolysis inhibitor and calcium channel regulator	chr16:66921678-66925644	2.33152	15.3715	2.72092	0.00015	0.0310521
ERG	ERG, ETS transcription factor	chr21:38379936-38661780	2.50476	0.260025	-3.26795	5.00E-05	0.0124559
ZC3H12A	zinc finger CCCH-type containing 12A	chr1:37474483-37484379	2.5178	27.5319	3.45087	5.00E-05	0.0124559
GRIP1	glutamate receptor interacting protein 1	chr12:66302444-66804186	2.86211	0.714187	-2.0027	5.00E-05	0.0124559
TNFAIP6	TNF alpha induced protein 6	chr2:151357591-151380048	3.10017	23.6116	2.92907	5.00E-05	0.0124559
RELB	RELB proto-oncogene, NF-kB subunit	chr19:45001429-45038194	3.24664	20.529	2.66064	0.0002	0.0397243
C15orf48	chromosome 15 open reading frame 48	chr15:45430528-45586304	3.46722	105.565	4.92821	5.00E-05	0.0124559
PARP12	poly(ADP-ribose) polymerase family member 12	chr7:140023743-140063721	3.60355	13.8702	1.94449	0.0001	0.0219373
TNFAIP3	TNF alpha induced protein 3	chr6:137823672-137883312	4.14814	70.1543	4.08	5.00E-05	0.0124559
AMPD3	adenosine monophosphate deaminase 3	chr11:10308312-10507579	4.21017	26.2652	2.6412	5.00E-05	0.0124559
IL7R	interleukin 7 receptor	chr5:35852694-35879603	4.50659	17.1924	1.93166	5.00E-05	0.0124559
PARK2	parkin RBR E3 ubiquitin protein ligase	chr6:161347419-163315492	4.96004	0.355266	-3.80338	5.00E-05	0.0124559
IL32	interleukin 32	chr16:3065296-3087100	5.05667	70.016	3.79143	5.00E-05	0.0124559
PARP14	poly(ADP-ribose) polymerase family member 14	chr3:122680617-122730840	5.07642	22.7363	2.16311	5.00E-05	0.0124559
IFI44	interferon induced protein 44	chr1:78649795-78664120	5.08599	46.6088	3.196	5.00E-05	0.0124559
GBP2	guanylate binding protein 2	chr1:89106131-89176040	5.13141	22.3103	2.12028	5.00E-05	0.0124559
IFI35	interferon induced protein 35	chr17:43006724-43014456	5.17351	28.7573	2.47471	0.00015	0.0310521
IRF1	interferon regulatory factor 1	chr5:132481608-132490798	6.28649	27.3311	2.12021	5.00E-05	0.0124559
CSF1	colony stimulating factor 1	chr1:109910241-109930993	6.46701	32.9044	2.34711	5.00E-05	0.0124559
PDPN	podoplanin	chr1:13583464-13617957	7.39325	54.5508	2.88332	5.00E-05	0.0124559
ABI3BP	ABI family member 3 binding protein	chr3:100749101-100993515	7.47862	44.1101	2.56027	5.00E-05	0.0124559
SLC43A3	solute carrier family 43 member 3	chr11:57386793-57427580	7.4997	31.6702	2.07822	0.0001	0.0219373
STC1	stanniocalcin 1	chr8:238419114-23854807	7.71336	36.4453	2.2403	0.0001	0.0219373
VCAM1	vascular cell adhesion molecule 1	chr1:100719741-100739045	8.47649	108.738	3.68125	5.00E-05	0.0124559
NFKB2	nuclear factor kappa B subunit 2	chr10:102394109-	8.71398	39.1334	2.167	5.00E-05	0.0124559

		102402529					
PAPPA	pappalysin 1	chr9:116153772-116402322	9.99727	36.9252	1.885	0.0001	0.0219373
CLDN1	claudin 1	chr3:190305700-190412143	10.022	66.4346	2.72876	0.00015	0.0310521
FHIT	fragile histidine triad	chr3:59749309-61251459	10.0362	0.959353	-3.38701	5.00E-05	0.0124559
PLSCR1	phospholipid scramblase 1	chr3:146513172-146544864	10.0403	33.624	1.7437	0.00025	0.0453642
MAN1A1	mannosidase alpha class 1A member 1	chr6:119177208-119349761	10.6771	40.7582	1.93258	5.00E-05	0.0124559
NAMPT	nicotinamide phosphoribosyltransferase	chr7:106248284-106286326	11.1375	70.6468	2.6652	5.00E-05	0.0124559
NAMPTL	nicotinamide Phosphoribosyltransferase Pseudogene 1	chr10:36521720-36524234	11.1467	50.7209	2.18596	5.00E-05	0.0124559
NFKBIA	NFKB inhibitor alpha	chr14:35401510-35404749	11.7044	92.9857	2.98996	5.00E-05	0.0124559
IL11	interleukin 11	chr19:55364359-55370463	11.7916	137.573	3.54437	5.00E-05	0.0124559
UBE2L6	ubiquitin conjugating enzyme E2 L6	chr11:57551655-57568284	12.5631	47.4698	1.91782	0.00025	0.0453642
ST7	suppression of tumorigenicity 7	chr7:116952445-117230103	13.0018	219.761	4.07915	5.00E-05	0.0124559
TFPI2	tissue factor pathway inhibitor 2	chr7:935915729-93911265	15.2534	150.608	3.30359	5.00E-05	0.0124559
CD82	CD82 molecule	chr11:44564426-44620363	17.2744	90.9421	2.39631	5.00E-05	0.0124559
C1R	complement C1r	chr12:7080208-7122501	17.7931	47.0554	1.40304	0.00025	0.0453642
LIF	leukemia inhibitory factor	chr22:30239193-30257441	17.9234	103.183	2.52528	5.00E-05	0.0124559
PPIF	peptidylprolyl isomerase F	chr10:79347468-79355337	18.2791	51.6866	1.4996	0.0002	0.0397243
NRP2	neuropilin 2	chr2:205681989-205798133	20.3695	73.5131	1.85159	5.00E-05	0.0124559
FAM84B	family with sequence similarity 84 member B	chr8:126552441-126713415	20.6608	4.82695	-2.09771	0.0001	0.0219373
NFKBIZ	NFKB inhibitor zeta	chr3:101779201-101861022	21.9384	60.2573	1.45768	0.00025	0.0453642
TNIP1	TNFAIP3 interacting protein 1	chr5:151029944-151093577	23.378	98.6386	2.077	5.00E-05	0.0124559
IFI6	interferon alpha inducible protein 6	chr1:27666060-27672218	25.2823	368.982	3.86735	5.00E-05	0.0124559
ISG15	ISG15 ubiquitin-like modifier	chr1:1001137-1014541	32.3332	323.06	3.32071	5.00E-05	0.0124559
SLC39A14	solute carrier family 39 member 14	chr8:22367248-22434129	35.661	182.218	2.35324	5.00E-05	0.0124559
PTX3	pentraxin 3	chr3:157175222-157533720	36.7351	280.721	2.93391	5.00E-05	0.0124559
SOD2	superoxide dismutase 2	chr6:159669056-159789749	39.0679	1280.35	5.03441	5.00E-05	0.0124559
AKR1B1	aldo-keto reductase family 1 member B	chr7:134442349-134459284	54.8537	236.928	2.11079	5.00E-05	0.0124559
JPX	JPX transcript, XIST activator (non-protein coding)	chrX:73944323-74293574	137.857	16.381	-3.07307	0.0001	0.0219373

ARIH2	ariadne RBR E3 ubiquitin protein ligase 2	chr3:48917787-49023495	159.733	29.1804	-2.45259	5.00E-05	0.0124559
PVT1_1	Pvt1 oncogene conserved region 1	chr8:127794485-128101253	426.305	29.0083	-3.87735	5.00E-05	0.0124559

[a]Benjamini-Hochberg adjusted p-value.

Supplementary Materials and methods

Astrocyte and tuberous sclerosis complex cell cultures

Briefly, after removal of blood vessels, tissue was mechanically minced into smaller fragments and enzymatically digested by incubating at 37˚C for 30 minutes with 2.5% trypsin (Sigma-Aldrich; St. Louis, MO, USA). Tissue was washed with incubation medium containing Dulbecco's modified Eagle's medium (DMEM)/HAM F10 (1:1) medium (Gibco, Thermo Fisher Scientific, Waltham, MA, USA), supplemented with 1% penicillin/streptomycin and 10% fetal calf serum (FCS; Gibco, Thermo Fisher Scientific, Waltham, MA, USA) and triturated by passing through a 70 µm mesh filter. Cell suspension was incubated at 37˚C, 5% CO2 for 48 hours to let astroglial cells adhere the culture flask before it was washed with phosphate-buffered saline (PBS; 0.1 M, pH 7.4) to remove excess of myelin and cell debris. Cultures were subsequently refreshed twice a week. Cultures reached confluence after 2-3 weeks. Secondary astrocyte cultures for experimental manipulation were established by trypsinizing confluent cultures and re-plating onto poly-L-lysine (PLL; 15 µg/ml, Sigma-Aldrich; St. Louis, MO, USA)-pre-coated 12 and 24-well plates (Costar, Cambridge, MA, USA; 10 × 104 cells/well in a 12-well plate for RNA isolation and quantitative real-time PCR; 5×10^4 cells/well in a 24-well plate for immunocytochemistry). For flow cytometric analysis, cells were plated at a density of 10×10^4 cells/well in uncoated 12-well plates. Astrocytes were used for analyses at passage 1-4. The purity of our cultures was examined using immunocytochemistry for GFAP, S100β and Vimentin, which showed approximately 98% purity.

Bioinformatics analysis of small RNA and mRNA-Seq data

Reads were aligned to the human reference genome, GRCh38 using TopHat2 v2.0.13, no mismatches between the trimmed reads and the reference genome were allowed, reads were allowed to be aligned a maximum of ten times (Kim et al. 2013). Using the featureCounts program from the Subread package the number of reads that aligned to the known miRNAs, according to miRBase21 (www.mirbase.org) and other short RNA species extracted from Gencode v25 were calculated (Griffiths-Jones 2004; Harrow et al. 2012; Liao et al. 2014). Small RNAs with less than 3 reads in 6 or more samples were excluded. Differential expression analysis was performed using DESeq2 (Love et al. 2014). The false discovery rate was controlled for using the Benjamini-Hochberg correction, gene expression changes with an adjusted p-value<0.05 were considered statistically significant.

References

Griffiths-Jones S. 2004. The microRNA Registry. Nucleic Acids Res 32:D109-11.

Harrow J, Frankish A, Gonzalez JM, Tapanari E, Diekhans M, Kokocinski F, Aken BL, Barrell D, Zadissa A, Searle S and others. 2012. GENCODE: the reference human genome annotation for The ENCODE Project. Genome Res 22:1760-74.

Kim D, Pertea G, Trapnell C, Pimentel H, Kelley R, Salzberg SL. 2013. TopHat2: accurate alignment of transcriptomes in the presence of insertions, deletions and gene fusions. Genome Biol 14:R36.

Liao Y, Smyth GK, Shi W. 2014. featureCounts: an efficient general purpose program for assigning sequence reads to genomic features. Bioinformatics 30:923-30.

Love MI, Huber W, Anders S. 2014. Moderated estimation of fold change and dispersion for RNA-seq data with DESeq2. Genome Biol 15:550.

SUPPLEMENTARY FIGURE 1: Relationship between C15orf48 and miR147b. The genomic location of C15orf48 and miR147b is shown. Both transcripts are transcribed from the same template strand on chromosome 15. The pre-miR147b transcript is harbored within a region that is also transcribed as the 3' UTR of C15orf48. There was a strong correlation between miR147b and C15orf48 expression levels (ρ=0.96, p-value<0.0001, Spearman's rank correlation test). Expression is shown in log2(normalized read-counts+1).

SUPPLEMENTARY FIGURE 2: miR147b expression in tuberous sclerosis complex (TSC) cortical tubers and temporal lobe epilepsy with hippocampal sclerosis (TLE-HS). Quantitative real-time PCR of fresh frozen brain tissue. **A** miR147b expression levels in TSC tubers (n=16) did not differ to expression in control cortex (n=19), however increased levels are observed in a subset of patients. **B** expression levels in TLE-HS (n=16) were increased compared to control hippocampus (n=14).

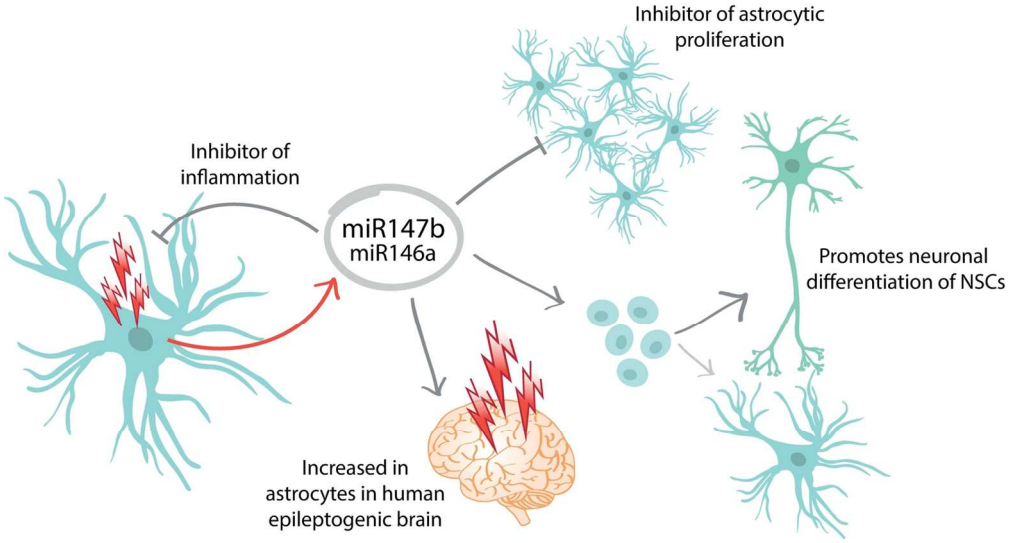

Table of Contents Image

141x75mm (300 x 300 DPI)